

On the heterogeneous electrical conductivity structure of the Earth's mantle with implications for transition zone water content

A. Khan,^{1,2} A. Kuvshinov,³ and A. Semenov³

Received 10 February 2010; revised 18 October 2010; accepted 2 November 2010; published 27 January 2011.

[1] We have investigated the lateral variations in mantle electrical conductivity structure using electromagnetic sounding data. For this purpose, we used very long time series (up to 51 years) of geomagnetic observatory data at six locations encompassing different geological settings to compute response functions that cover the broadest possible frequency range (3.9 to 95.2 days): Fürstenfeldbrück (FUR), Europe; Hermanus (HER), South Africa; Langzhou (LZH), China; Alice Springs (ASP), Australia; Tucson (TUC), United States (North America); and Honolulu (HON), United States (North Pacific). We inverted the response functions beneath each observatory for a local radial conductivity profile using a stochastic sampling algorithm. Specifically, we found significant lateral variations in conductivity throughout the mantle with resolution limited to the depth range ~500–1200 km. At 600 km depth, conductivity varies between 0.1 and 0.4 S/m and increases to 1.3–2.0 S/m at 800 km depth beneath all stations except HER (0.5 S/m). At 900 km depth, conductivity increases further to 1.4–2.4 S/m with HER, HON, and ASP being most conductive. This trend persists to a depth of 1200 km. Comparison with conductivity profiles constructed from laboratory measurements of mantle mineral conductivities and models of Earth's mantle composition and thermal state reveal that significant thermochemical variations are at the origin of the observed heterogeneities in mantle conductivity found here. Because of the somewhat large error bounds on sampled conductivity profiles and the reduced sensitivity of the electromagnetic sounding data above 500 km depth, constraints on transition zone water content are less conclusive, although H₂O contents <0.5 wt% in the midtransition zone appear less likely.

Citation: Khan, A., A. Kuvshinov, and A. Semenov (2011), On the heterogeneous electrical conductivity structure of the Earth's mantle with implications for transition zone water content, *J. Geophys. Res.*, 116, B01103, doi:10.1029/2010JB007458.

1. Introduction

[2] Lateral and radial variations in mantle composition are believed to be due to the processes that occur at midocean ridges, where differentiation of peridotitic mantle produces an oceanic lithosphere that is physically and chemically stratified into a basaltic crust and its depleted complement, harzburgite [e.g., Ringwood, 1975; Hofmann, 1997]. At subduction zones, meanwhile, the oceanic lithosphere is cycled back into the mantle, where buoyancy forces can produce a radial variation in the amount of subducted crust, including segregation of the basaltic component toward the base of the mantle, as suggested by mantle convection

simulations [e.g., Christensen and Hofmann, 1994; Xie and Tackley, 2004; Nakagawa *et al.*, 2009]. These and other geophysical studies, including seismology and seismic tomography studies in particular, reveal a mantle with a variety of heterogeneous structures persisting at all length scales [e.g., Helffrich and Wood, 2001; Becker and Boschi, 2002; Panning and Romanowicz, 2006; Kustowski *et al.*, 2008], bearing evidence of the complex dynamics that have shaped mantle structure. In spite of many advances, seismology has yet to provide a clear picture of the origin of the large-scale heterogeneities [e.g., Trampert and Van der Hilst, 2005].

[3] An alternative means of addressing mantle heterogeneity is to investigate properties that, in principle, are more sensitive to parameters such as composition and temperature than is elasticity. One such property is electrical conductivity, which is what we shall be concerned with here. Electrical conductivity of mantle minerals measured in the laboratory is found to depend strongly on temperature and composition, and hence mineralogy [e.g., Tyburczy and Fiesler, 1995]. The electrical conductivity of olivine, for

¹Niels Bohr Institute, University of Copenhagen, Copenhagen, Denmark.

²Institute of Geochemistry and Petrology and Institute of Geophysics, Swiss Federal Institute of Technology, Zurich, Switzerland.

³Institute of Geophysics, Swiss Federal Institute of Technology, Zurich, Switzerland.

example, changes by at least two orders of magnitude as it transforms to wadsleyite at around 400 km depth [e.g., *Xu et al.*, 1998]. For this reason, electrical conductivity is a potentially strong tool for mapping mantle chemistry and physical structure and presents a complementary method to seismic studies that seek to elucidate the elastic properties of the mantle. For example, and in spite of present uncertainties in measured mineral electrical conductivities, *Xu et al.* [2000a], *Dobson and Brodholt* [2000a], and *Khan et al.* [2006] showed that conductivities of mantle minerals measured in the laboratory are consistent with the geophysical data (e.g., electromagnetic response functions of *Olsen* [1999]) and moreover that the results can be used to discriminate between different mantle geotherms and compositions.

[4] Inversion of long-period electromagnetic (EM) sounding data from ground-based geomagnetic observatories or orbiting satellites has over the years provided insight into the electrical conductivity structure of the Earth, mainly as global or semi-global one-dimensional (1D) radial profiles [e.g., *Olsen*, 1999; *Utada et al.*, 2003; *Constable and Constable*, 2004; *Kuvshinov et al.*, 2005; *Kuvshinov and Olsen*, 2006; *Martinec and Velimsky*, 2009; *Velimsky*, 2010]. In these models, electrical conductivity generally increases as a function of depth from the base of the lithosphere throughout the transition zone (TZ) and down to a depth of about 1000 km. The maximum depth to which these models are constrained is around 1500 km because of the limited frequency range (≤ 1 yr) of the electromagnetic sounding data. Conductivities in the upper part of the lower mantle reach ~ 1 S/m, which are consistent with laboratory-measured conductivities for the major lower-mantle minerals magnesiowüstite and perovskite [e.g., *Shankland et al.*, 1993; *Katsura et al.*, 1998; *Xu et al.*, 1998; *Dobson and Brodholt*, 2000b].

[5] Since variations in conductivity with mineralogy are much stronger than the corresponding variations in elastic properties, tomography-like images based on electrical conductivity obviously present an intriguing prospect for unraveling the nature of mantle heterogeneities. Lateral variations in conductivity have been reported on the basis of regionalized studies [e.g., *Schultz and Larsen*, 1987, 1990; *Schultz*, 1990; *Egbert and Booker*, 1992; *Schultz et al.*, 1993; *Lizzaralde et al.*, 1995; *Neal et al.*, 2000; *Ichiki et al.*, 2001; *Jones et al.*, 2003; *Tarits et al.*, 2004; *Ledo and Jones*, 2005], and from a number of full three-dimensional (3D) semiglobal [*Fukao et al.*, 2004; *Koyama et al.*, 2006; *Utada et al.*, 2009; *Shimizu et al.*, 2010] and global 3D conductivity inversions [*Kelbert et al.*, 2009; A. Kuvshinov and A. Semenov, Global 3-D imaging of mantle conductivity based on inversion of ground-based *C*-responses: I. An approach and its verification, manuscript and preparation, 2010; A. Semenov and A. Kuvshinov, Global 3-D imaging of mantle conductivity based on inversion of ground-based *C*-responses: II. Results, manuscript in preparation, 2010].

[6] In the present study, we continue the effort of retrieving information on the global mantle conductivity structure. We pay particular attention to data analysis, as the procurement of a set of internally consistent and coherent response functions is singularly important, and as will become clear is far from an easy task, for studies seeking to investigate the Earth's 3D conductivity structure from geomagnetic observatory data. In the following, we detail a scheme by which

data are first subjected to various corrections and then inverted. The data corrections include accounting for the effects of ocean induction, remote reference techniques, and other issues, such as violation of assumed source geometry and then inverted. We follow the approaches of, e.g., *Schultz* [1990] and *Neal et al.* [2000] and consider data from six observatories distributed across the globe (Europe, South Africa, China, Australia, North America, and North Pacific) and invert the corrected data from each observatory for a local 1D radial electrical conductivity profile, which provides insight into the large-scale heterogeneous conductivity features of the Earth. With regard to making 3D inferences from 1D radial conductivity profiles, we specifically discuss the feasibility of doing so by showing that the response of a 3D model constructed from our inverted 1D radial profiles is entirely in agreement with the responses obtained from 1D models only. Moreover, by comparing results obtained here with laboratory-based conductivity models that rely on the most recent laboratory conductivity measurements for major TZ minerals in combination with self-consistently computed mineralogical mantle models, we will learn what implications can be drawn from EM sounding data with regard to compositional and thermal variations, and not least TZ water content.

[7] As concerns the inverse problem, we employ the Bayesian approach formulated by *Tarantola and Valette* [1982] and *Mosegaard and Tarantola* [1995]. With this approach, the solution is presented in terms of a large collection of models sampled from the posterior distribution in the model space using a Markov chain Monte Carlo algorithm. While this algorithm is based on a random sampling of the model space, only models that result in a good data fit and are consistent with prior information are frequently sampled.

2. Data Selection and Processing

[8] To construct *C*-responses (defined below), we selected data on the basis of the following four interdependent criteria: (1) We acquired *C*-responses for different regions of the world where a quasi-1D behavior of the responses is expected. We thus excluded from consideration regions where the subsurface conductivity structure is potentially influenced by complex 3D features such as subduction zones. (2) We gathered *C*-responses from observatories located far away from the polar regions, where auroral source effects are known to influence the results [*Fujii and Schultz*, 2002]. (3) We obtained *C*-responses that are characterized by low uncertainty and high coherency and that vary smoothly. (4) We collected *C*-responses covering the broadest possible period range. As a result of an intensive search, we decided upon data (hourly mean values) from the following six geomagnetic observatories that satisfy the above criteria: Fürstfeldbrück (FUR), Europe; Hermanus (HER), South Africa; Langzhou (LZH), China; Alice Springs (ASP), Australia; Tucson (TUC), United States, North America; and Honolulu (HON), United States, North Pacific. Geographic and geomagnetic coordinates of these observatories and the length of data series considered are summarized in Table 1.

[9] To estimate *C*-responses from irregular variations caused by large-scale magnetospheric sources, it is commonly assumed that the source field potential for these variations is proportional to the first zonal harmonic, P_1^0 , in

Table 1. Summary of Geomagnetic Observatories

Station	Latitude	Longitude	Geomagnetic	Observation
			Latitude	Period
Fürstfeldbrück (FUR)	48.17	11.28	48.38	1957–2007
Hermanus (HER)	−34.43	19.23	−33.98	1957–2007
Langzhou (LZH)	36.09	103.85	25.86	1980–2007
Alice Springs (ASP)	−23.76	133.88	−32.91	1992–2007
Tucson (TUC)	32.17	249.27	39.88	1957–1994
Honolulu (HON)	21.32	202.00	21.64	1961–2007

the geomagnetic coordinate system. On the basis of this assumption about source structure, it is possible to derive the C -responses from magnetic measurements at a given site as follows [Banks, 1969]:

$$C(\omega) = -\frac{a \tan \vartheta}{2} \frac{Z(\omega)}{H(\omega)}, \quad (1)$$

where $a = 6371.2$ km is the mean radius of the Earth, ϑ is the geomagnetic colatitude, $Z(\omega)$ and $H(\omega)$ are the vertical and horizontal (directed toward geomagnetic north) components of the geomagnetic field, respectively, at frequency $\omega = 2\pi/T$, where T is the period. This technique is called the $Z:H$ method, and the five-step procedure described below details how we estimated C -responses from the raw observatory data.

[10] 1. We remove the secular variation from the original time series of the magnetic field. For each component, secular variation is treated by means of cubic B-splines with a knot separation of 2 years.

[11] 2. The resulting time series of the horizontal component are rotated into dipole coordinate system related to the 1950 epoch.

[12] 3. Segments of Z and H time series of length $3T_i$ (hereinafter called *realizations*) are prepared for estimating time harmonics of Z and H at various periods T_i , $i = 1, \dots, N$, with N being the number of considered periods. To increase the number of realizations, successive realizations overlap 50% with preceding realizations. If a given realization contains gaps in either component (Z or H), we exclude it from further analysis. To reduce side lobes, a Hamming window is also applied to each realization.

[13] 4. C -responses are estimated as follows:

$$C = -\frac{a \tan \vartheta}{2} \frac{\langle ZWH^* \rangle}{\langle HWH^* \rangle}, \quad (2)$$

where H^* is the complex conjugate of H , and $\langle \dots \rangle$ denotes summation over all realizations. Non-Gaussian noise is handled with an iterative robust weight W (a form of Huber weights), which reduces the effect of outliers. The corresponding errors are calculated as follows [Schmucker, 1999]:

$$\delta C(\omega) = |C| \sqrt{\frac{1 - \text{coh}^2}{\text{coh}^2} \left(\frac{1}{\beta}\right)^{\frac{1}{m}}}, \quad (3)$$

where $m = N - 1$ and N is the number of realizations for a specific period, while $1 - \beta$ is the confidence level, i.e., the probability that modulus $|C|$ lies within error limits $|C| \pm \delta C$. In our calculations, the confidence level is chosen to be 0.9.

We also tried modern robust nonparametric methods for deriving errors [Chave and Thomson, 2004] and found that both methods as applied to good-quality data (by definition of our selection criteria) give errors of similar size. Squared coherence coh^2 is calculated as follows:

$$\text{coh}^2 = \frac{|\langle ZWH^* \rangle|^2}{\langle ZWZ^* \rangle \langle HWH^* \rangle}. \quad (4)$$

As examples, we display observed C -responses for the South African observatory HER in Figure 1 and the European observatory FUR in Figure 2. A few common features can be noted. First, in the period range between 1.5 days (1.3×10^5 s) and 110 days (9.5×10^6 s), the responses demonstrate smooth behavior, low uncertainty, and high coherence (the latter is especially true for observatory HER). Second, at periods shorter than 1.5 days, the responses are scattered and not very coherent. This is not surprising, since variations at these periods are mostly caused by electric currents in the ionosphere that have a very different spatiotemporal source structure than magnetospheric sources. Finally, at periods longer than 110 days, the responses are again seen to be scattered, and in the period range from 110 to 220 days (1.9×10^7 s), a minimum in the real part of the C -responses is observed. This is incompatible with the assumption of a 1D conductivity structure for which, as an example, the following inequality has to be fulfilled [Weidelt, 1972, p. 11]:

$$\frac{d \text{Re}\{C\}}{d \log T} \geq 0. \quad (5)$$

This behavior hints at either violation of the P_1^0 source-structure assumption in the above period range and/or contamination from the core. The uncertainty at longer periods increases as a result of a decrease in the number of realizations. On the basis of these considerations, in addition to our requirement that squared coherency coh^2 should be larger than 0.6, we decided to use only responses in the period range between 3.9 and 95.2 days in our analysis.

[14] With regard to the use of equation (2) to estimate C -responses, the question of a possible downward bias of the latter has to be addressed. For this purpose, we calculate responses using the remote reference technique [Gamble et al., 1979], which allows a reduction of downward bias of the C -response estimates (should this bias exist). The responses are computed as follows:

$$C = -\frac{a \tan \vartheta}{2} \frac{\langle ZWH_{\text{ref}}^* \rangle}{\langle HWH_{\text{ref}}^* \rangle}, \quad (6)$$

where H_{ref}^* are realizations at the reference observatory, which is sufficiently far away so that noise sources in H and H_{ref} are independent. Applying this technique, we found that estimates calculated with the use of equations (2) and (6) are very similar for all observatories over the period range of interest. We note that we tried to pair each observatory with different possible reference observatories, but noticed only a negligible difference between the different estimates so computed. This is illustrated in Figure 3, which shows the results of C -response estimates for FUR computed using equations (2) and (6). Circles depict the results obtained from

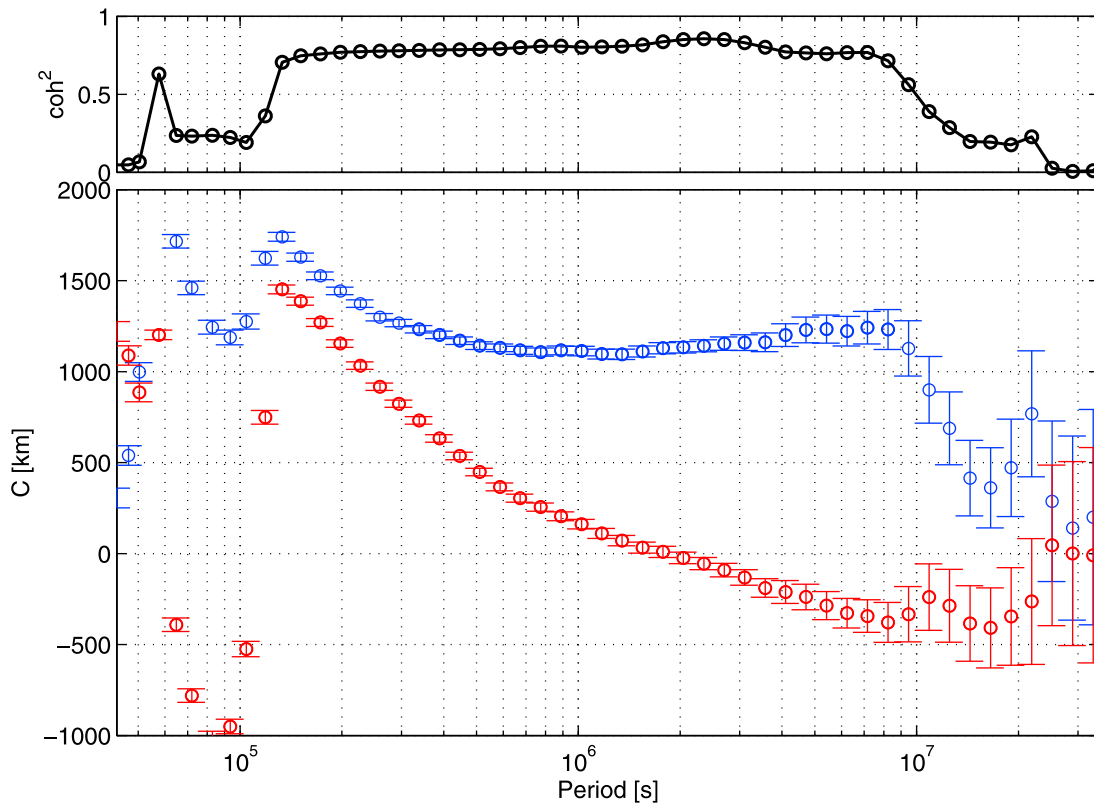


Figure 1. Observed C -responses for the South African observatory HER for periods between 12 hours and 400 days (blue, $\text{Re}\{C\}$; red, $\text{Im}\{C\}$). Squared coherency is shown in black.

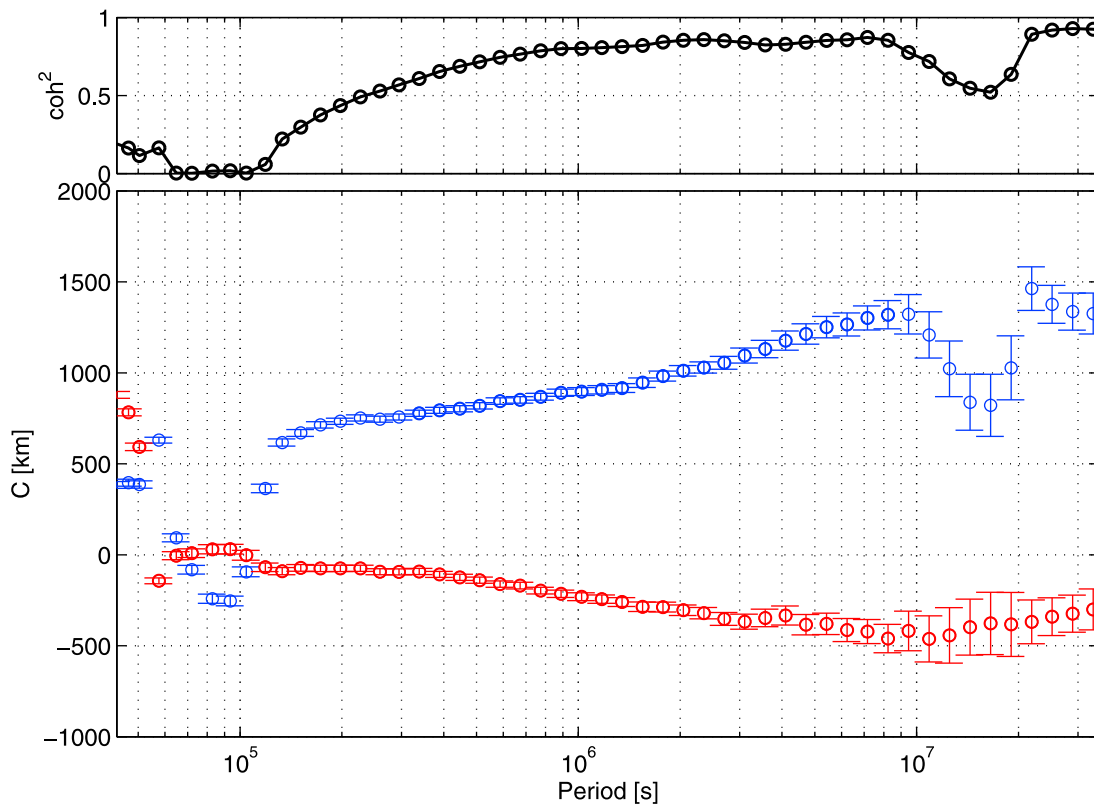


Figure 2. Same as Figure 1 for the European observatory FUR.

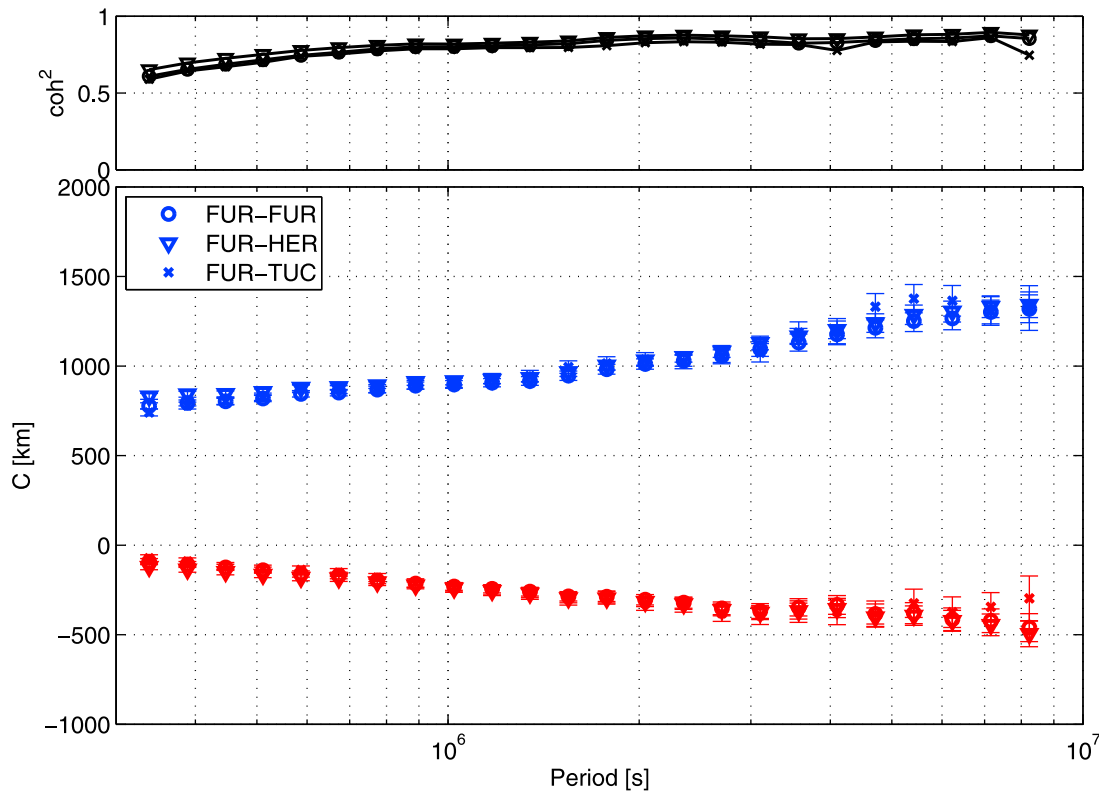


Figure 3. Comparison of C -responses for the European observatory FUR estimated with the use of equations (2) and (6) (for details, see main text). Period range is 3.9 to 95.2 days. Circles signify the results obtained from “single site” estimation (using equation (2)), and triangles and crosses denote the results obtained using remote reference technique (see equation (6)) with HER (South Africa) and TUC (North America) as respective reference observatories. As in Figure 1, blue, $\text{Re}\{C\}$; red, $\text{Im}\{C\}$.

“single site” estimation (i.e., using equation (2)), triangles and crosses denote the results obtained using the remote reference technique (equation (6)), employing HER and TUC as remote reference observatories. The responses are seen to be very close over the whole period range considered, which suggests that the signal-to-noise ratio in the horizontal component is rather low and that the use of equation (2) for obtaining unbiased estimates of the C -response is appropriate.

[15] 5. The final issue to be addressed concerns correcting the observed C -responses for the ocean effect. In Figure 1, we observe that the response for the coastal observatory HER shows an extremely strong anomalous effect, which manifests itself as a deviation of the observed response from that of a 1D conductivity structure. This is evident for periods shorter than 15 days (1.3×10^6 s), where a violation of the inequality (equation (5)) for the real part of the C -response is particularly noticeable. Moreover, for periods shorter than 24 days (2×10^6 s), the imaginary part of the response appears to be positive, which is in contradiction with the behavior expected from a 1D conductivity model, as it should be negative. These observations contrast with the results from the inland observatory FUR (see Figure 2), where the response is seen to be in overall agreement with that of a 1D model. The major contributor to the anomalous behavior of C -responses at coastal observatories was shown

by *Kuvshinov et al.* [2002] to originate in a nonuniform ocean. *Kuvshinov et al.* [2002] also showed that the effects arising from the oceans may be corrected for by multiplying the observed response, C , by the ratio of the synthetic response of a spherically symmetric conductive Earth (without oceans), C^{1D} , with the response of the same spherically symmetric conductive Earth overlaid by an inhomogeneous shell (shell approximates the nonuniform oceans), $C^{1D+shell}$,

$$C^{corr}(\omega) = C(\omega) \times \frac{C^{1D}(\omega)}{C^{1D+shell}(\omega)}. \quad (7)$$

Utada et al. [2003] suggested an iterative correction process based on the aforementioned procedure of *Kuvshinov et al.* [2002] and showed that, with a few iterations, good agreement between observed and predicted responses for coastal observatories in the North Pacific region is achieved. Applying this iterative correction to the data from station HER, we took as our starting point a plausible 1D conductivity model. Employing equation (7), we obtained a corrected set of responses and inverted these using a stochastic sampling algorithm (to be discussed in section 4). With the new 1D model (most probable), we made another correction (equation (7)) and reinverted these corrected responses. This process was repeated until a satisfactory fit between the response predicted by successive models with nonuniform

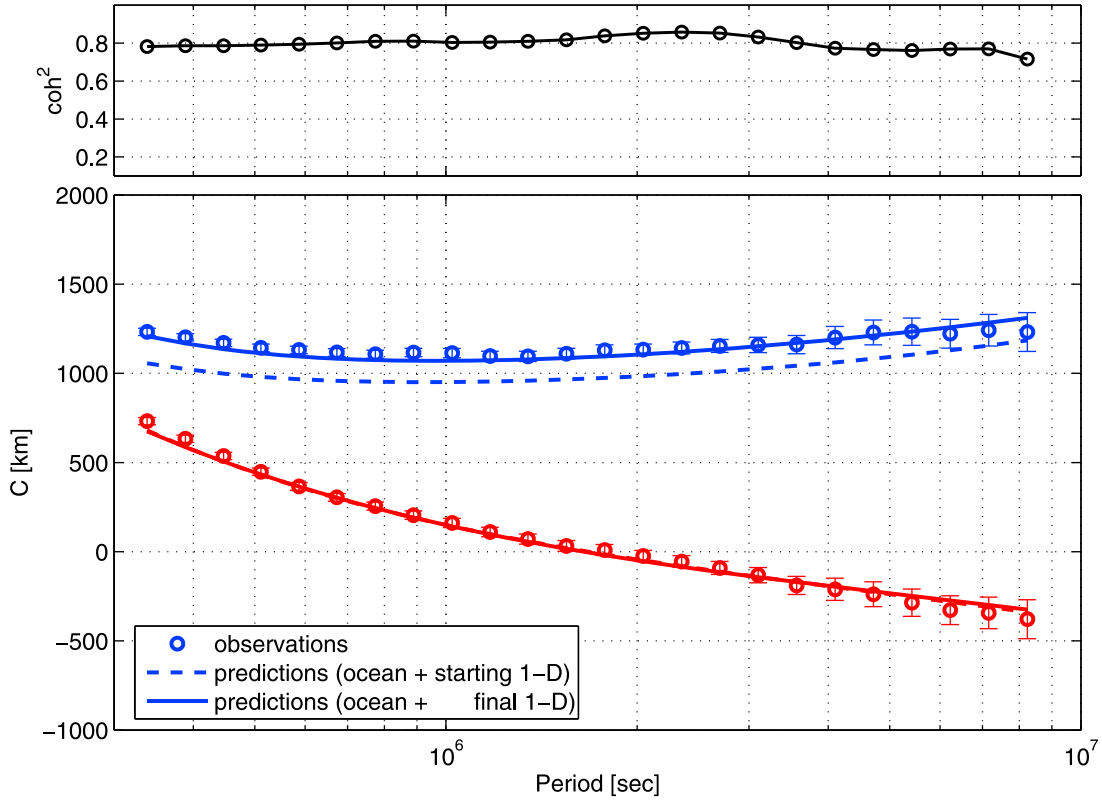


Figure 4. Observed and predicted C -responses for the South African observatory HER after application of the iterative correction (see text for details). Circles with error bars, observations; dashed line, predictions using 1D starting model; solid line, predictions after third (final) correction. As in Figure 1, blue, $\text{Re}\{C\}$; red, $\text{Im}\{C\}$.

oceans and the observed response was achieved. We applied this iterative correction to the data from HER and found that after three iterations, the predicted responses agreed well with the observed response (see Figure 4). By performing calculations in the models with and without oceans, we also investigated whether the responses at the remaining five observatories were distorted by the ocean effect. We found that only the response at the TUC observatory was influenced, although to a much lesser degree than observed at HER. In spite of this, we applied the iterative correction to the data from TUC and obtained good agreement between predictions and observations after the two iterations.

[16] For both observatories, we used as starting 1D conductivity model a four-layer Earth model (similar to that described by *Schmucker* [1985a]). It consists of a 100 km resistive lithosphere of $3000 \Omega\text{m}$ followed by a moderately resistive first layer of $70 \Omega\text{m}$ down to 500 km, a second transition layer of $16 \Omega\text{m}$ from 500 km to 750 km, and a central uniform sphere of $0.42 \Omega\text{m}$.

3. Forward Problem: Prediction of C -Responses

[17] Prediction of C -responses relies on calculating the magnetic fields induced in the specified spherical conductivity model of the Earth by a given time-varying source. Assuming that the considered sources can be converted into the frequency domain by Fourier transformation, the

magnetic (and electric) fields, $\mathbf{H}(\mathbf{E})$, obey Maxwell's equations

$$\nabla \times \mathbf{H} = \sigma \mathbf{E} + \mathbf{j}^{\text{ext}}, \quad (8)$$

$$\nabla \times \mathbf{E} = -i\omega\mu_0 \mathbf{H}, \quad (9)$$

where \mathbf{j}^{ext} is the inducing (given) source (in our case, magnetospheric ring current), $i = \sqrt{-1}$, σ is the specified conductivity distribution of the model and μ_0 is the magnetic permeability of free space. We assume a time dependence of the form $\exp i\omega t$. Above the conducting Earth ($r > a$) and beneath the magnetospheric source, the Fourier component of the magnetic field, $\mathbf{B} = \mu_0 \mathbf{H} = -\nabla V$, can be derived from a scalar magnetic potential, V , which is represented by a spherical harmonic expansion

$$V = a \sum_{n=1}^{\infty} \sum_{m=-n}^n \left[\epsilon_n^m(\omega) \left(\frac{r}{a}\right)^n + l_n^m(\omega) \left(\frac{a}{r}\right)^{n+1} \right] P_n^m(\cos \vartheta) e^{im\varphi}, \quad (10)$$

where r , ϑ , φ are the distance from the Earth's center, colatitude and longitude (in the geomagnetic coordinate system), respectively, ϵ_n^m and l_n^m are the complex expansion coefficients of the external (inducing) and internal (induced) parts of the potential, and $P_n^m(\cos \vartheta)$ are associated Legendre

polynomials of degree n and order m . The inducing current \mathbf{j}^{ext} in equation (8) can be considered in the form of a spherical harmonic expansion of equivalent sheet currents. These are assumed to flow in a shell at $r = a$ (embedded in an insulator) and to produce the external magnetic field exactly

$$\mathbf{B}^{\text{ext}} = -\nabla V^{\text{ext}}, \quad (11)$$

with the external potential given by

$$V^{\text{ext}} = a \sum_{n=1}^{\infty} \sum_{m=-n}^n \epsilon_n^m(\omega) \left(\frac{r}{a}\right)^n P_n^m(\cos \vartheta) e^{im\varphi}, \quad (12)$$

at the Earth's surface $r = a$. In this case, the equivalent sheet current, \mathbf{J}^{ext} , can be written in the following form [Schmucker, 1985b]:

$$\mathbf{J}^{\text{ext}} = \frac{\delta(r-a)}{\mu_0} \sum_{n=1}^{\infty} \sum_{m=-n}^n \frac{2n+1}{n+1} \epsilon_n^m \mathbf{e}_r \times \nabla_{\perp} (P_n^m(\cos \vartheta) e^{im\varphi}), \quad (13)$$

where \mathbf{e}_r is a radially outward pointing unit vector, δ is Dirac's delta function, \times denotes a vector product, and ∇_{\perp} is the angular part of the gradient. In our case, the model is excited by a large-scale, symmetric—with respect to the geomagnetic equator—ring current, and thus the sheet current density reduces to the following:

$$\mathbf{J}^{\text{ext}} = -\frac{3}{2} \epsilon_1^0 \sin \vartheta \mathbf{e}_{\varphi} \delta(r-a) / \mu_0. \quad (14)$$

Assuming that the conductivity model of the Earth is in the form of a layered sphere with constant conductivity within each layer, one can obtain recurrence formulae from equations (8) and (9) to predict C -responses at various frequencies (for details, the reader is referred to, e.g., Srivastava [1966] and Schmucker [1970]). These recurrence formulae have been used in the frame of our Monte Carlo inversion.

[18] To calculate responses in a model with 3D conductivity distributions (for example, in the model with non-uniform oceans (1D + shell)), the numerical solution of Kuvshinov [2008], which is based on an integral equation approach, has been employed.

4. Inversion of C -Responses

4.1. Formulation and Solution of the Inverse Problem

[19] For a general inverse problem, the relationship between model \mathbf{m} and data \mathbf{d} is usually written as follows:

$$\mathbf{d} = \mathbf{g}(\mathbf{m}), \quad (15)$$

where \mathbf{g} is a typically nonlinear operator. Central to the formulation of the Bayesian approach to inverse problems as delineated by Tarantola and Valette [1982] is the extensive use of probability density functions (*pdfs*) to describe any piece of information that enters the problem. These *pdfs* include (1) probabilistic prior information on model and data parameters, $\rho(\mathbf{m})$ (for the present brief discussion, we limit ourselves to a functional dependence on \mathbf{m} and omit any reference to \mathbf{d}), and (2) the physical laws that relate data to the model parameters which are sought.

[20] These *pdfs* are then combined using Bayes theorem to yield the posterior *pdf* $\Sigma(\mathbf{m})$ in the model space

$$\Sigma(\mathbf{m}) = k\rho(\mathbf{m})\mathcal{L}(\mathbf{m}), \quad (16)$$

where k is a normalization constant and $\mathcal{L}(\mathbf{m})$ is the likelihood function, which in probabilistic terms can be interpreted as a measure of misfit between observed data and data calculated from model \mathbf{m} . Prior information and the likelihood function are dealt with in section 4.3.

4.2. MCMC Sampling of the Posterior Distribution

[21] Having defined the posterior distribution above (equation (16)) as the solution to our inverse problem, let us turn to the problem of actually obtaining $\Sigma(\mathbf{m})$. In the case of the general inverse problem, however, the posterior *pdf* does not exist as an analytical function, and, given its usually complex shape defined over a high-dimensional model space, it cannot be integrated analytically. Instead, we have to estimate posterior probabilities by statistical integration methods, and the basic idea is to design a random walk in the model space that, if unmodified, samples some initial probability distribution. By subsequently applying certain probabilistic rules, we can modify the random walk in such a way that it will sample some target distribution. The Metropolis-Hastings algorithm [Metropolis *et al.*, 1953; Hastings *et al.*, 1970] is a Markov chain Monte Carlo (MCMC) method which can be shown to be the one that most efficiently achieves this goal. The MCMC method is so named because it employs a random number generator (Monte Carlo) and has the shortest possible memory, that is, each step is dependent only upon the previous step (Markov chain). This is contained in the following algorithm [e.g., Mosegaard, 1998].

[22] Algorithm. *If we have a random function $\mathcal{K}(\mathbf{m}^n)$ which samples the prior probability density $\eta(\mathbf{m})$ iteratively $\mathbf{m}^{n+1} = \mathcal{K}(\mathbf{m}^n)$, and a random function \mathcal{F} generating a uniformly distributed random number from the interval $[0,1]$, the random function Ξ , which iteratively operates on the current parameter vector \mathbf{m}^n and produces the next parameter vector \mathbf{m}^{n+1}*

$$\mathbf{m}^{n+1} = \Xi(\mathbf{m}^n) = \begin{cases} \mathcal{K}(\mathbf{m}^n) & \text{if } \mathcal{F} \leq \min\left[1, \frac{\mathcal{L}(\mathcal{K}(\mathbf{m}^n))}{\mathcal{L}(\mathbf{m}^n)}\right], \\ \mathbf{m}^n & \text{else.} \end{cases}$$

samples the probability density $\sigma(\mathbf{m}) = k\eta(\mathbf{m})\mathcal{L}(\mathbf{m})$.

[23] In addition, \mathcal{K} has to satisfy the following two constraints: (1) given enough iterations, access to all points \mathbf{m} in the parameter space must be ensured through the iterative procedure, and (2) successive visits (or more) to the same point are possible, i.e., $\mathbf{m}^n = \mathcal{K}(\mathbf{m}^n)$.

[24] Of importance here is that this algorithm renders us capable of sampling the space with a sampling density proportional to the given probability density without excessively sampling low-probability areas of the model space. This is especially important when we are concerned with high-dimensional spaces, where a large proportion of the volume may have near-zero probability density. It might be noted that exhaustive sampling, where all points in a dense grid covering the model space are visited in a random fashion, is

the simplest method, but is inappropriate for problems with more than 10 parameters [Tarantola, 2004, p. 49] and thus most geophysical applications.

[25] The solution to the general inverse problem as presented here is generally best described by looking at samples from the posterior *pdf* rather than studying single realizations such as the mean, the median model, or the maximum likelihood model. One possibility is to calculate resolution measures, which are easily evaluated from the following equation [e.g., Mosegaard, 1998]:

$$\mathcal{R}(\mathcal{E}, f) = \int_{\mathcal{E}} f(\mathbf{m}) \Sigma(\mathbf{m}) d\mathbf{m} \approx \frac{1}{N} \sum_{\{\mathbf{m}_n \in \mathcal{E}\}} f(\mathbf{m}_n) \quad (17)$$

where $f(\mathbf{m})$ is a given function of the model parameters \mathbf{m} , \mathcal{E} is an event or subset of the model space containing the models of current interest, and N is the total number of samples taken from \mathcal{E} .

4.3. Sampling the Prior and Posterior Distributions

4.3.1. Prior Information

[26] We consider a spherical Earth varying laterally and radially in properties. At each geographical point of interest we represent our local model of the Earth by a number of layers of varying conductivity and thickness. We have divided our model of the Earth into 26 layers of fixed thickness (at intervals of 25 km in the depth range 0–100 km and 100 km in the depth range 100–2000 km, while the remaining three layers are placed at 2300, 2600, and 2891 km depth, respectively), and each of these layers is further parameterized by an electrical conductivity value. This particular parameterization, although somewhat coarse, was chosen as it was found to provide an adequate fit to the data. We tried several other parameterizations, including ones with higher as well as lower radial resolution. Reducing the number of layers typically resulted in an inability to fit data, whereas increasing the number of layers does not improve the data fit much beyond that of our 26-layer model. In summary, the resolution adopted here was found on the grounds that the distribution of calculated data provided an adequate fit to the observed data distribution and at the same time resulted in relatively narrow model parameter uncertainties.

[27] The electrical conductivity in a given layer i is determined from $\sigma_i = \sigma_{i-1} + \alpha \cdot (\sigma_{i+1} - \sigma_{i-1})$, where α is a uniformly distributed random number in the interval [0,1], with no upper limit but a lower limit set on σ_i at the surface ($\sigma_i = 5 \times 10^{-4}$ S/m). The latter condition is imposed because the data have low sensitivity to the highly resistive lithosphere. Other choices resulted in no measurable changes. This method of estimating σ ensures that electrical conductivity is a nondecreasing function with depth, as is expected on the basis of values of electrical conductivities of mantle minerals measured in the laboratory and conductivity models deduced from these values [Xu et al., 2000a; Dobson and Brodholt, 2000a; Khan et al., 2006]. Given that the EM sounding data considered here have resolution only down to a depth of 1400 km, we fixed core conductivity to 5×10^5 S/m in accordance with Stacey and Anderson [2001]. In summary, the inverse problem consists of 26 parameters in all.

4.3.2. Posterior Information

[28] Assuming that data noise follows a Gaussian distribution, the likelihood function is computed from:

$$\mathcal{L}(\mathbf{m}) \propto \exp \left(- \sum_i \frac{[i d_{\text{obs}}^{\text{Re}\{C\}} - i d_{\text{cal}}^{\text{Re}\{C\}}(\mathbf{m})]^2}{2_i \Delta_{\text{Re}\{C\}}^2} + \frac{[i d_{\text{obs}}^{\text{Im}\{C\}} - i d_{\text{cal}}^{\text{Im}\{C\}}(\mathbf{m})]^2}{2_i \Delta_{\text{Im}\{C\}}^2} \right), \quad (18)$$

where $d_{\text{obs}}^{\text{Re}\{C\}}$, $d_{\text{obs}}^{\text{Im}\{C\}}$, $d_{\text{cal}}^{\text{Re}\{C\}}$, and $d_{\text{cal}}^{\text{Im}\{C\}}$ denote observed and calculated real and imaginary C -responses, respectively, and $\Delta_{\text{Re}\{C\}}$ and $\Delta_{\text{Im}\{C\}}$ denote the uncertainties of either of these.

[29] In each iteration, all conductivity parameters from the surface and down to the core mantle boundary were perturbed using the proposal (i.e., prior) distribution as defined above. The adopted proposal distribution has a burn-in time (i.e., convergence time) of the order of 1000 iterations, after which retention of samples commences. In all, 10 million models were sampled, and, to ensure near-independent samples, every 1000th model was retained for further analysis, with an overall acceptance rate of 32%.

[30] In relation to the inverse problem, the advantage of the probabilistic approach lies in its ability to fully incorporate nonlinearities into the final solution, obviating any form of linearization of the original problem and thus providing more realistic error limits to the results for a given resolution. In solving inverse problems, we face the usual trade-off between resolution and uncertainty, which is largely determined by the chosen parameterization. Finally, it should be clear that the *pdfs* calculated here are based on the quantitative information which has been used as input in the inversion. Stated differently, the probabilities that we calculate are based entirely on (1) data and their uncertainties, (2) prior information as quantified here, and (3) the physical relation between data and model parameters.

[31] In the present statistical treatment of the general inverse problem, Mosegaard and Tarantola [1995] considered covariance matrices as inadequate descriptors of model resolution and model parameter uncertainties, and they advocated the movie strategy as a reasonably direct means of conveying information on these measures. This strategy essentially amounts to displaying a collection of models from the prior and posterior *pdfs*, which, when compared visually, enables us to distinguish features that are well resolved from those that are less well resolved. Prior and posterior information is summarized in Figure 5, which shows 45 models taken randomly from the prior and posterior *pdfs*, respectively. For example, all posterior models reveal increases in conductivity between 600–800 km depth. Model parameter variance, resolution, correlation, or any other measures of interest can be analyzed quantitatively through the use of equation (17).

5. Results and Discussion

5.1. Electrical Conductivity Structure

[32] The inverted (posterior) electrical conductivity structure beneath the six observatories is shown in Figures 6b–6d,

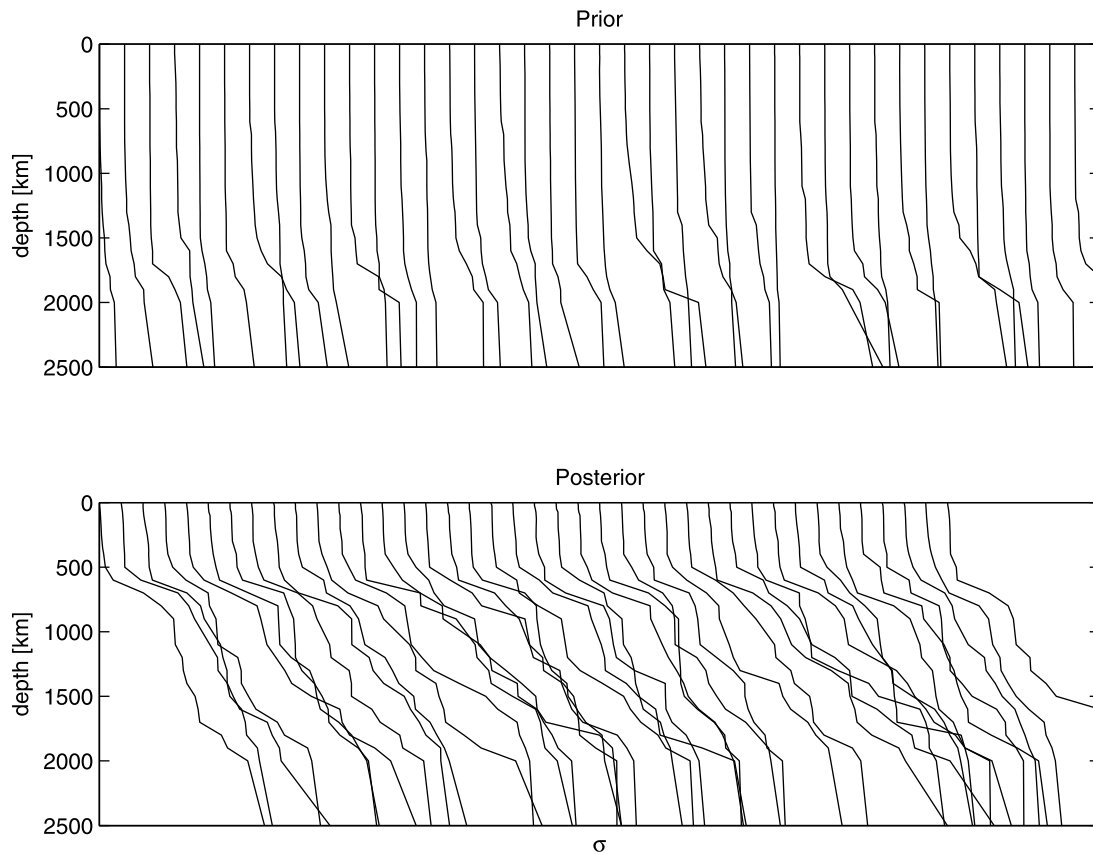


Figure 5. Forty-five conductivity models taken from the (top) prior and (bottom) posterior probability distributions. Horizontal separation between models is 0.5 S/m.

together with prior models (Figure 6a), as 95% credible intervals (the credible interval is defined as the shortest possible interval containing a given probability), while their predicted responses are shown in Figure 7. First, we note the difference in the general appearance of prior and posterior models; not only are posterior *pdfs* displaced relative to the prior ones, but they are also significantly narrower in the depth range shown here. The latter observation directly reflects the amount of information contained in the data. While posterior plots appear displaced relative to prior plots over the entire depth range shown, an increase in model variability in the range of ~ 400 – 700 km is nonetheless apparent, which, in spite of the differences between prior and posterior *pdfs* reflects reduced data sensitivity in the upper TZ. As a result, we show only models in the depth range 400–1200 km, and although it appears that conductivity structure in the upper and mid-TZ are constrained, we caution the reader against interpreting conductivity at these depths. In summary, there is generally good resolution in the depth range ~ 600 – 1200 km, whereas conductivities above and below this level are less well constrained. This somewhat conservative estimate contrasts to some extent with the results of *Utada et al.* [2009], whose EM sounding data in the period range 5–50 days (compared with ~ 4 –95 days here) were inverted for TZ conductivity structure in the depth range 400–700 km. Our interpretation of data sensitivity is also consistent with the penetration depths that we deduce from Figure 7, as the value of $\text{Re}\{C\}$ at a given

period is roughly a measure of the depth to which the corresponding EM field penetrates [*Weidelt*, 1972].

[33] For comparison, we are also showing some previously obtained models in Figure 6 from the European study of *Olsen* [1999] and the global study of *Kuvshinov and Olsen* [2006]. The former model is based on responses derived from geomagnetic observatories, while the latter derives from responses of orbiting satellite data. Two features are characteristic of these models: (1) the model of *Kuvshinov and Olsen* is more conductive over the entire depth range, and (2) both models increase in conductivity in a continuous fashion from the upper to the midmantle. Unlike the laboratory-based models of *Xu et al.* [2000a] and *Khan et al.* [2006], and unlike seismological models in general, none of the models presented in Figure 6 show strong discontinuities around 410 and 660 km depth, where important mineral phase transformations take place (olivine to wadsleyite and ringwoodite to perovskite and magnesiowüstite, respectively). Our profiles, like those of most previous studies, are characterized by a continuous increase in conductivity throughout the upper mantle, TZ, and upper part of the lower mantle, reflecting the diffusive nature of EM fields and their diminished sensitivity to discontinuous material properties. The inability of EM fields to sense discontinuities in material properties explains why models with and without jumps in conductivity are equally good at resolving data, as noted by, e.g., *Neal et al.* [2000] in their study of long-period magnetotelluric and geomagnetic depth

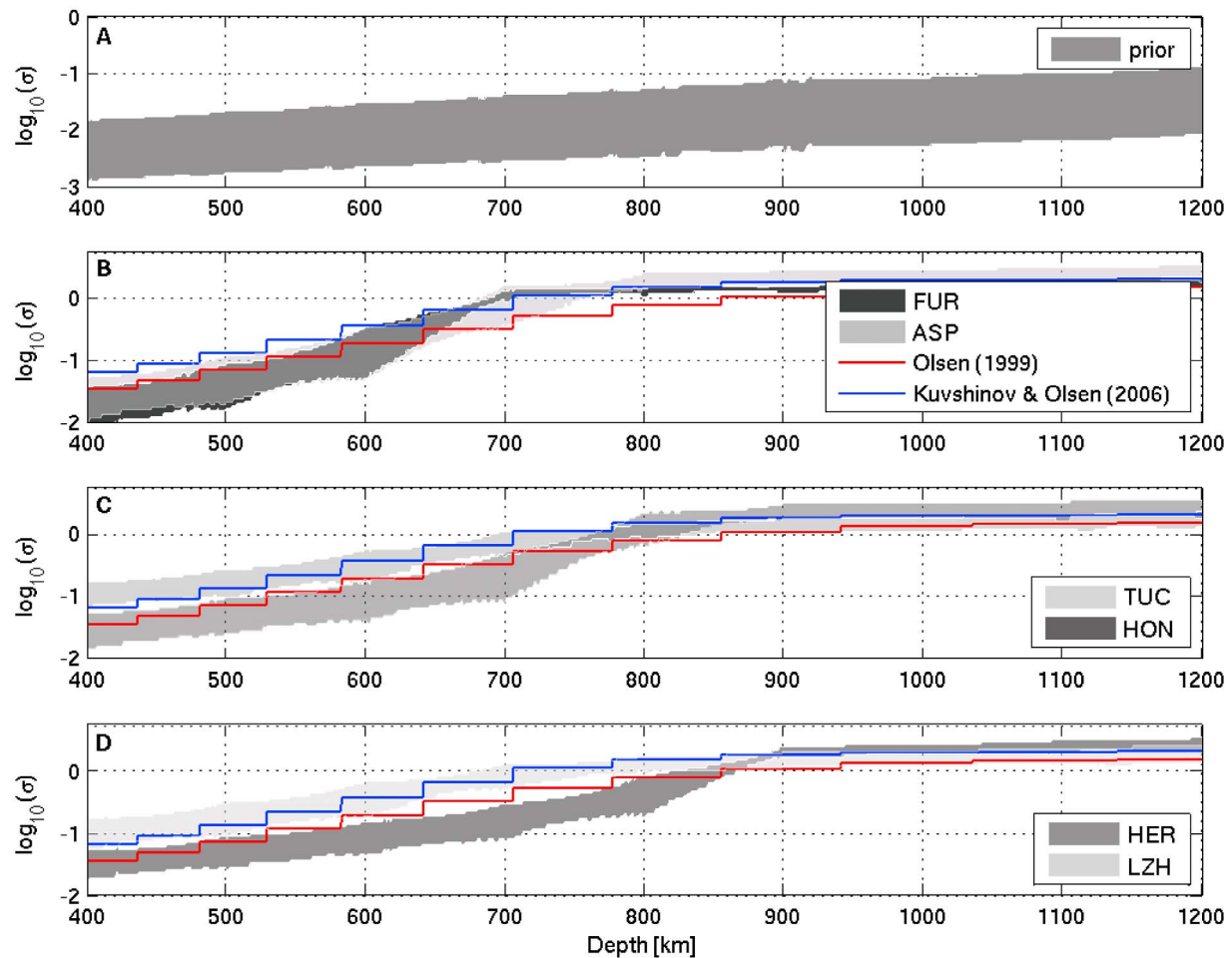


Figure 6. Credible intervals (95%) of sampled (a) prior and (b–d) posterior models in the depth range 400–1200 km. For comparison, two previous one-dimensional conductivity models are indicated by colored lines.

sounding data beneath HON, TUC, Midway (Pacific), and Carty Lake (Canada). Models with and without strong discontinuities marking the upper and lower mantle transition were found to fit data equally well (see also discussion in the next section). Incidentally, their inverted models underneath HON and TUC are analogous to ours in that TUC is more conductive than HON over the depth range 400–1000 km.

[34] In the upper part of the lower mantle, differences between conductivity profiles beneath the observatories are particularly noticeable (see Figure 6). At a depth of 600 km, conductivities are seen, within their uncertainties, to overlap with values varying between 0.1 and 0.4 S/m. Below the TZ, conductivities increase beneath most stations to values ranging from 1.2 to 2.0 S/m, except for HER, which remains relatively resistive at ~ 0.5 S/m. In the range 900–1100 km depth, conductivities increase to values ranging from 1.4 to 2.6 S/m, with stations FUR, TUC, and LZH having conductivities < 2 S/m, while stations ASP, HON, and HER are characterized by higher values (> 2 S/m). In comparison to earlier models, we find that the model of *Kuvshinov and Olsen* [2006] is in good agreement with our results, in particular for depths > 900 km, whereas the model of *Olsen* [1999] is barely within the limits of our models, except

beneath TUC. Mantle conductivity values found here are summarized in Table 2.

[35] Mid- and lower-mantle conductivity structure, i.e., depth range 1500–2900 km, is not constrained by data. However, if we assume that conductivity continues to increase linearly and extrapolate our profiles, conductivities in the range 5–10 S/m are obtained, in accord with recent measurements of the electrical conductivity of postperovskite at lowermost mantle conditions [*Ohta et al.*, 2008].

[36] The localities analyzed here are representative of a number of different tectonic settings, covering regions of continental extension (TUC), ocean (HON), relatively young continents (FUR and HER), and the stable Archean Australian craton (ASP). Evidence provided by seismic tomography images reveal [e.g., *Panning and Romanowicz*, 2006; *Kustowski et al.*, 2008] significant differences in seismic wave velocities between continental and oceanic regions extending to depths of ~ 200 –250 km, while such differences tend to be smoothed out once depth ranges of present interest are reached. This behavior is somewhat analogous to what is found here, in particular in the upper part of the lower mantle (> 900 km depth), where the variation of retrieved conductivity profiles is significantly diminished in

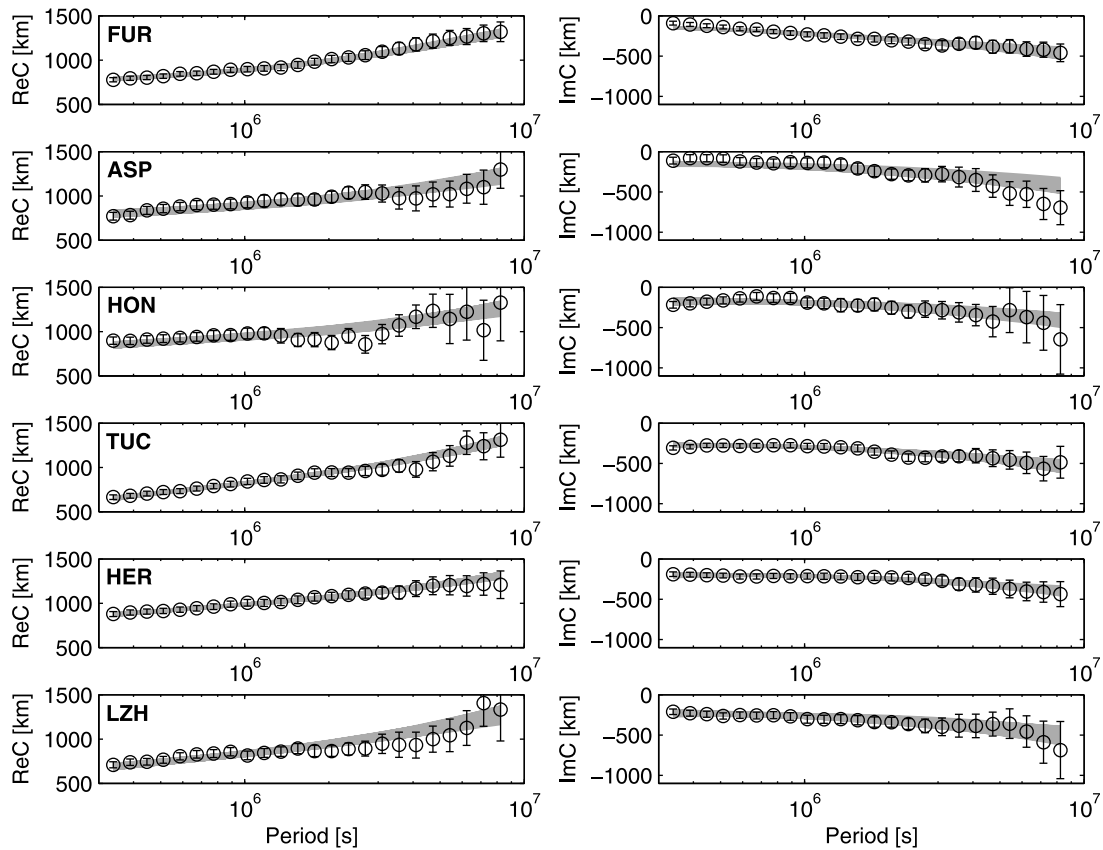


Figure 7. Data fit for the six observatories. (left) $\text{Re}\{C\}$ and (right) $\text{Im}\{C\}$, with gray lines being data predicted from the models in Figure 6. Circles and bars indicate observed data and uncertainties.

comparison to the upper mantle. In the regions covering the lower part of the TZ and uppermost lower mantle (depth range $\sim 600\text{--}900$ km), however, palpable differences are discernible. Similar results were found in the global model of *Kelbert et al.* [2009] and to some extent in the regional study by *Neal et al.* [2000]. Global differences at such depths, particularly in the lower TZ, likely reflect concomitant variations in temperature, composition, water, and possibly melt content.

5.2. Validity of One-Dimensional Approach

[37] In the present section, we assess whether the interpretation of our local 1D profiles in terms of 3D structure is feasible. We tested this by constructing a 3D mantle conductivity model by spline interpolation of the most probable 1D conductivity model at each of the six sites and overlaying this with a surface shell. We computed the response from this 3D model as well as responses from a model with a surface shell and local 1D structure underneath. As expected, responses calculated using the 3D model are found to be very similar at all sites to those calculated using the model with a surface shell and local 1D structure underneath. This is illustrated in Figure 8, which summarizes these results for observatory TUC. It is seen that the difference between the responses calculated from a full 3D model (labeled “3D+ocean” in Figure 8) and the responses calculated in a 1D model overlaid by a nonuniform shell (labeled “1D+ocean” in Figure 8) is negligible.

[38] To further assess the validity of the 1D nature of our results, we inverted our C -responses at the six stations (note that for HER and TUC, corrected responses were inverted) using the D+ algorithm of *Parker and Whaler* [1981]. At all sites, we found the normalized misfit of the optimal 1D conductivity model to be less than the expectation value of 1, thus supporting local one-dimensionality of the responses in the considered period range. Moreover, we also checked a set of Weidelt’s inequalities [*Weidelt*, 1972, p. 11], which 1D responses have to fulfill. The inequalities were also found to be satisfied for most of the data with sporadic (also visible in Figure 7) deviations, which we attribute either to shortcomings of the data analysis or to some inconsistency of the external field model. These model studies, along with the observation that experimental C -responses (corrected responses for HER and TUC and initial responses for the remaining four observatories) overall reveal 1D behavior (cf. Figure 7), are evidence in support of the use of our 1D profiles for making inferences

Table 2. Summary of Mean Mantle Conductivities (in S/m) and Uncertainties

Depth	FUR	ASP	HON	TUC	HER	LZH
600	0.2 ± 0.1	0.2 ± 0.1	0.1 ± 0.04	0.3 ± 0.1	0.1 ± 0.03	0.4 ± 0.1
800	1.4 ± 0.1	2.0 ± 0.3	1.5 ± 0.4	1.2 ± 0.2	0.5 ± 0.2	1.3 ± 0.2
900	1.5 ± 0.1	2.2 ± 0.3	2.4 ± 0.4	1.4 ± 0.2	2.1 ± 0.2	1.6 ± 0.3
1100	1.6 ± 0.2	2.4 ± 0.4	2.6 ± 0.4	1.6 ± 0.2	2.5 ± 0.3	1.7 ± 0.3

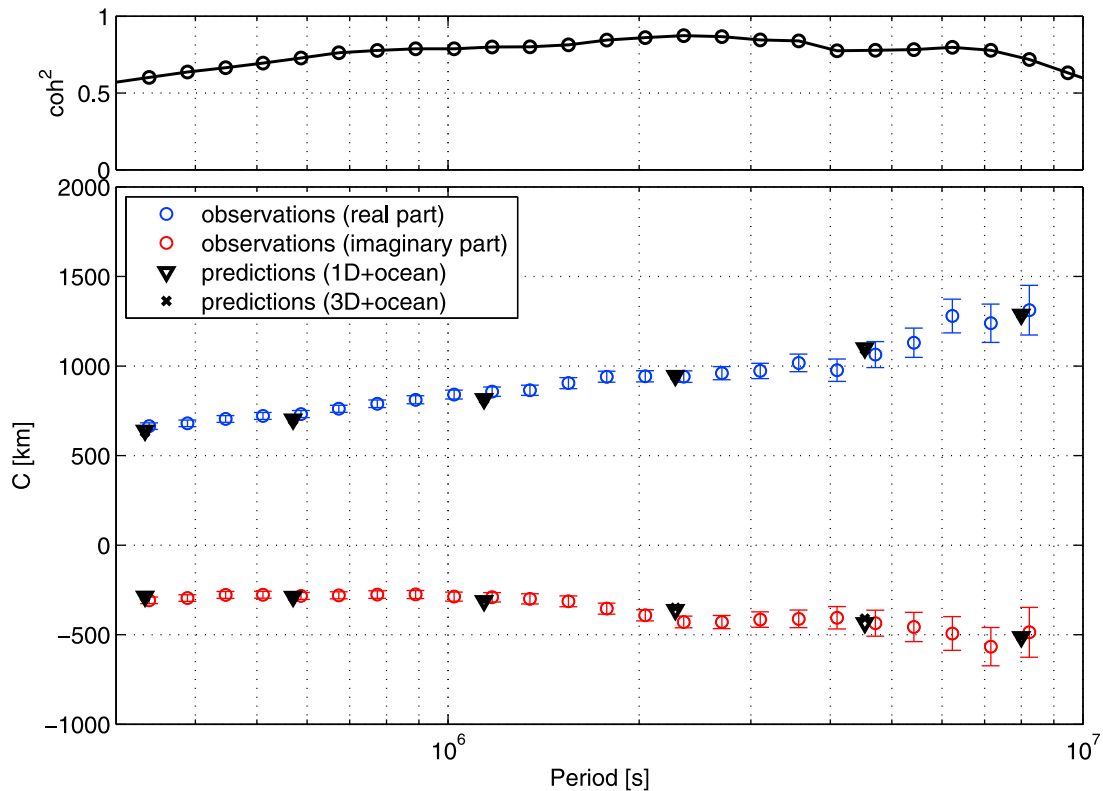


Figure 8. Comparison of observations with predictions obtained from “3D+ocean” and “1D+ocean” models for the North American observatory TUC. Observed C -responses are shown in blue ($\text{Re}\{C\}$) and red ($\text{Im}\{C\}$), while the responses calculated using the 3D model constructed on the basis of our inverted 1D profiles (see main text for details) are indicated by crosses and the responses calculated on the basis of a 1D model overlaid by a nonuniform shell are indicated by inverted triangles.

on a global scale. It should be borne in mind, however, that a certain bias is implicit in our model since we excluded from consideration regions where the subsurface conductivity structure is potentially influenced by complex 3D features such as subduction zones.

5.3. Laboratory-Based Electrical Conductivity Models and Transition Zone Water Content

[39] Electrical conductivity is highly sensitive to the presence of water in mantle minerals [e.g., Karato, 1990], which, even in small amounts, holds the potential of changing their physical properties [Hirth and Kohlstedt, 1996; Karato and Jung, 1998], with implications for the dynamics of the mantle [Bercovici and Karato, 2003]. Thus, the question of the amount and distribution of water in the mantle is of great interest, in particular that which might be stored in the TZ, as laboratory measurements have shown that the major TZ minerals wadsleyite and ringwoodite are highly water-soluble [Inoue et al., 1995; Kohlstedt et al., 1996]. Recent laboratory experiments have extended early measurements of the electrical conductivity of wadsleyite (Wads) and ringwoodite (Ring) to conditions appropriate for the TZ and confirmed the sensitive nature of the electrical conductivity of these minerals to water content [Huang et al., 2005; Yoshino et al., 2008;

Manthilake et al., 2009; Dai and Karato, 2009]. On the basis of these data, it should in principle be possible to infer mantle water content from a quantitative comparison of geophysically derived conductivity profiles and the laboratory data just discussed. Given the somewhat limited depth range sampled presently, we are only able to infer water content in the lower TZ (≥ 600 km).

[40] The comparison hinges on the construction of a reliable laboratory-based conductivity profile, and in doing so, we follow the approach of our previous study [Khan et al., 2006], where laboratory data were combined with a self-consistently computed mineralogical model of the Earth’s mantle from a specific composition and geotherm using Gibbs free energy minimization [Connolly, 2005]. Laboratory electrical conductivity measurements for the most important upper, TZ, and lower mantle minerals are summarized in Figure 9a (accounting for variations in temperature, pressure, and composition). The data compiled in Figure 9a are taken from Yoshino et al. [2006] for olivine (Ol), from Xu and Shankland [1999] for orthopyroxene (Opx) and clinopyroxene (Cpx), from Yoshino et al. [2008b] for garnet (Gt), from Manthilake et al. [2009] for Wads, from Yoshino et al. [2008a] and Yoshino and Katsura [2009a] for Ring, from Xu et al. [2000a] for wustite (Wus), and from Xu et al. [1998] for perovskite (Pv). Although we presently use only the measurements of Yoshino and coworkers for

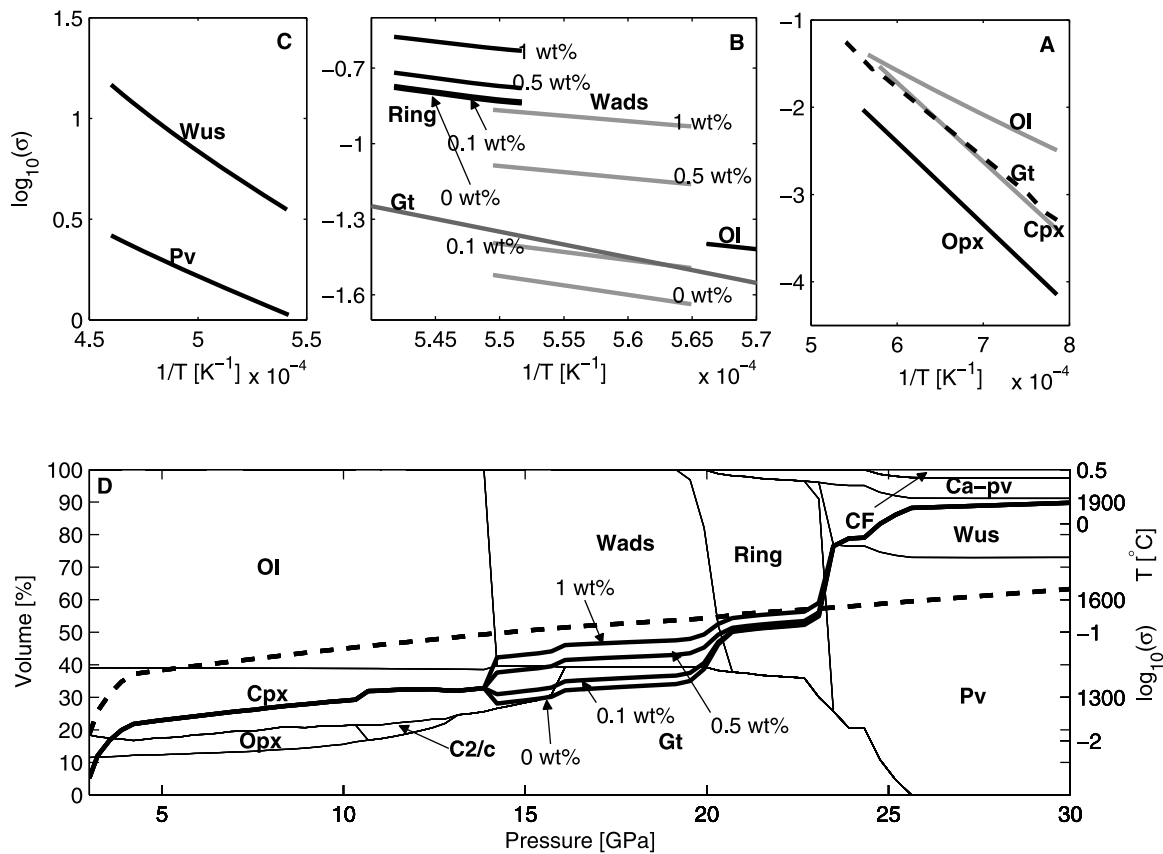


Figure 9. Laboratory mineral electrical conductivity measurements as a function of inverse temperature. (a) Upper mantle. (b) Transition zone. (c) Upper part of lower mantle. (d) Variations in mineral phase proportions and laboratory-based conductivity profile computed on the basis of a homogeneous adiabatic pyrolite mantle as a function of pressure (depth) and transition zone water content are shown in Figures 9b and 9d. The solid and dotted lines in Figure 9d are bulk conductivity and adiabat, respectively. Phases are Ol (olivine), Opx, (orthopyroxene), Cpx (clinopyroxene), C2/c (high-pressure Mg-rich Cpx), Gt (garnet), Wads (wadsleyite), Ring (ringwoodite), Aki (akimotoite), Ca-pv (calcium perovskite), Wus (magnesiowüstite), Pv (perovskite), and CF (calcium ferrite). See main text for further discussion.

hydrous Wads and Ring, we have to acknowledge that experimental disagreement currently exists with regard to the electrical conductivity of these minerals. *Dai and Karato* [2009] independently measured the conductivity of the major TZ minerals as a function of temperature and water content and obtained results that differ from those of Yoshino and coworkers. The ensuing discussion [see, e.g., *Karato and Dai*, 2009; *Yoshino and Katsura*, 2009b; *Yoshino*, 2009] has not been able to resolve the disagreements, and the controversy remains. Given the ready applicability of Yoshino and coworkers' results [e.g., *Manthilake et al.*, 2009, equation (6)], we resorted to employing these data here and leave it for a future study to consider the implications of *Dai and Karato's* [2009] measurements.

[41] Phases not considered here include C2/c (the high-pressure polymorph of Cpx), calcium ferrite (CF) and calcium perovskite (Ca-pv), for which no measurements presently are available. However, as these phases are present at levels <10 vol%, which are too small to materially affect bulk conductivity, we follow *Xu et al.* [2000a] and omit their contributions to the total rock conductivity. For exam-

ple, we found that disregarding C2/c in the upper mantle (assuming that the conductivity of C2/c is equal to that of Cpx) amounted to a difference in bulk conductivity of <0.02 log units. For present purposes, we assume a compositionally homogeneous mantle of pyrolitic composition along the adiabatic geotherm of *Brown and Shankland* [1981]. Equilibrium mineralogy so computed is shown in Figure 9b. The bulk electrical conductivity as a function of depth and water content (solid lines in Figure 9b) for this mineral assemblage is then obtained by combining the mineral phase proportions with the laboratory-measured mineral conductivities shown in Figure 9a at the appropriate physical conditions (temperature and pressure) and composition (Fe variation in Ring). To average the contribution from single minerals, we employed the geometrical mean as suggested by *Shankland and Duba* [1990] and also employed in our previous work [*Khan et al.*, 2006]. Alternative averaging schemes include the Hashin-Shtrikman extremal bounds [e.g., *Jones et al.*, 2009].

[42] In constructing the conductivity profile, we made a number of assumptions. In the upper mantle and TZ, we

omitted contributions arising from activation volume, relying on the results reported by *Xu et al.* [2000b], who showed that the electrical conductivity of olivine is independent of pressure. Although *ten Grotenhuis et al.* [2004] claimed to have found evidence for a grain boundary transport affecting the electrical properties of fine-grained olivine, we also disregard their contributions here, given the failure of others in finding systematic variations in conductivity with grain size [e.g., *Roberts and Tyburczy*, 1991; *Xu et al.*, 2000a]. TZ minerals are stable only over a relatively narrow depth range, and effects of pressure on the electrical conductivity of Wads and Ring are also likely to be less important. The electrical conductivities of Ring for various water contents shown in Figure 9a also consider effects of variation in Fe content as implicitly measured by *Yoshino and Katsura* [2009a]. However, as we are considering only a single composition, no changes related to variations in Fe are seen. For the lower mantle, we rely on the earlier measurements as summarized by *Xu et al.* [2000a], considering effects of activation volume and thus pressure, but disregarding compositional effects arising from variations in Al [see *Xu et al.*, 1998] and Fe [see *Dobson and Brodholt*, 2000]. As concerns oxygen fugacity in the upper mantle and TZ, we follow *Yoshino et al.* [2008] and consider data for polycrystalline olivine on a MoMoO₂ buffer, while oxygen fugacity in the TZ is taken to be equal to iron-wüstite. For the lower mantle, no adjustments for oxygen fugacity are implemented as the latter still remains to be determined.

[43] Noticeable features of the laboratory-based conductivity profile shown in Figure 9b are the jumps in conductivity associated with the major mineralogical phase transitions: at ~14 GPa Ol transforms to Wads (the seismic 410 km discontinuity), at ~21 GPa Wads transforms to Ring (the seismic 520 km discontinuity) and then again at the transition to the lower mantle (~23.5 GPa), where Ring transforms to Wus and Pv (the seismic 660 km discontinuity). The magnitudes of both transitions Ol→Wads and Ring→Wus+Pv are seen to depend strongly on water content. For a dry mantle, conductivity even drops on going from Ol to Wads, which is related to the combined presence of the higher conductivity phases Cpx and Gt relative to dry Wads. A water content of 0.15 wt% is needed so that conductivity in the top of the TZ equals that of the lowermost upper mantle. Discontinuous jumps in conductivity associated with the transitions from the upper mantle to the TZ and from the TZ to the lower mantle are not observed in our inverted profiles or in any of the previous global [*Kuvshinov and Olsen*, 2006], continental European [*Olsen*, 1999], and regional profiles, including the northeast Pacific [*Lizzaralde et al.*, 1995], Pacific [*Kuvshinov et al.*, 2005], Philippine Sea [*Seama et al.*, 2007], Carty Lake [*Neal et al.*, 2000], and Slave Craton [*Jones et al.*, 2003], with the exception of maybe the superior province study by *Schultz et al.* [1993], where a discrete conductivity jump in the depth range 416–456 km was identified. All aforementioned studies, including the present one, are characterized by a continuous increase in conductivity throughout the upper mantle, TZ, and upper part of the lower mantle. This reflects the diffusive nature of EM fields and their diminished sensitivity to discontinuities in material properties as discussed earlier, thereby complicating quantitative comparison between

geophysically derived and laboratory-based conductivity models. Only through a more definitive approach where *C*-response estimates are inverted in combination with the mineral physics database do conductivity jumps associated with the major phase transitions unambiguously appear [e.g., *Xu et al.*, 2000a; *Khan et al.*, 2006]. Finally, and although the presence of water likely stabilizes Wads over Ol [e.g., *Wood*, 1995], we omitted this in computing the phase equilibria shown in Figure 9b because of the scarcity of relevant data.

[44] We have displayed our conductivity and the laboratory-based profiles in Figure 10. The latter are shown as colored lines and include, in addition to effects arising from varying water content, variations in conductivity related to thermal variations. It is apparent that varying temperatures by 100°C changes conductivity by ~0.3 log units, whereas the change associated with varying water content from 0 to 1 wt% is ~0.4–0.6 log units. Note that variation in conductivity due to changes in water content is influenced by temperature. “Hotter” conditions tend to diminish the conductivity variations arising from changes in water relative to “colder” conditions. Figure 9b shows that the relative difference in conductivity of Wads and Ring decreases markedly as water content increases. Also apparent from the laboratory-based profiles are depth variations of the transformations Ol→Wads and Wads→Ring, which move up under “colder” conditions, in agreement with what was found for a descending slab [e.g., *Bina and Helffrich*, 1994]. The depth at which Ring transforms to Wus+Pv is seen to be essentially unchanged.

[45] For comparison, we have also added the laboratory-based conductivity profiles of *Xu et al.* [2000a], *Khan et al.* [2006], and *Yoshino et al.* [2008a] in Figure 10. The two former models are based on the laboratory mineral electrical conductivity database summarized in *Xu et al.* [2000a]. Marked differences between earlier and present models (note that previous models displayed in Figure 10 relate only to dry conditions) are seen to occur at the locations of the major transitions, i.e., Ol→Wads, Wads→Ring, and Ring→Wus+Pv. In previous models, the magnitude of the conductivity jump at which Ol→Wads is much larger than modeled presently, while those related to the transformations of Wads→Ring and Ring→Wus+Pv are diminished. These differences are easily understood as arising from the use of a different set of mineral conductivity data. Comparing our present model to the model of *Yoshino et al.* [2008a], which is based partly on the same data employed here (both without water), conductivity increases are in somewhat better agreement (compare 0.8 log units at “520” with 0.5 log units found here and 0.5 log units at “660” with 0.7 log units obtained here), although differences at the Ol→Wads transition still persist. These remaining discrepancies derive from the fact that *Yoshino et al.* [2008a] do not consider a realistic mineralogical model for the mantle in constructing their conductivity profile.

[46] The large variability in sampled conductivity profiles shown in Figure 10, spanning about 0.5 log units and thus essentially the same range encompassed by varying water content from 0 to 1 wt%, makes it difficult to draw any firm conclusions about the latter. The inherent trade-off that exists between water content and temperature further

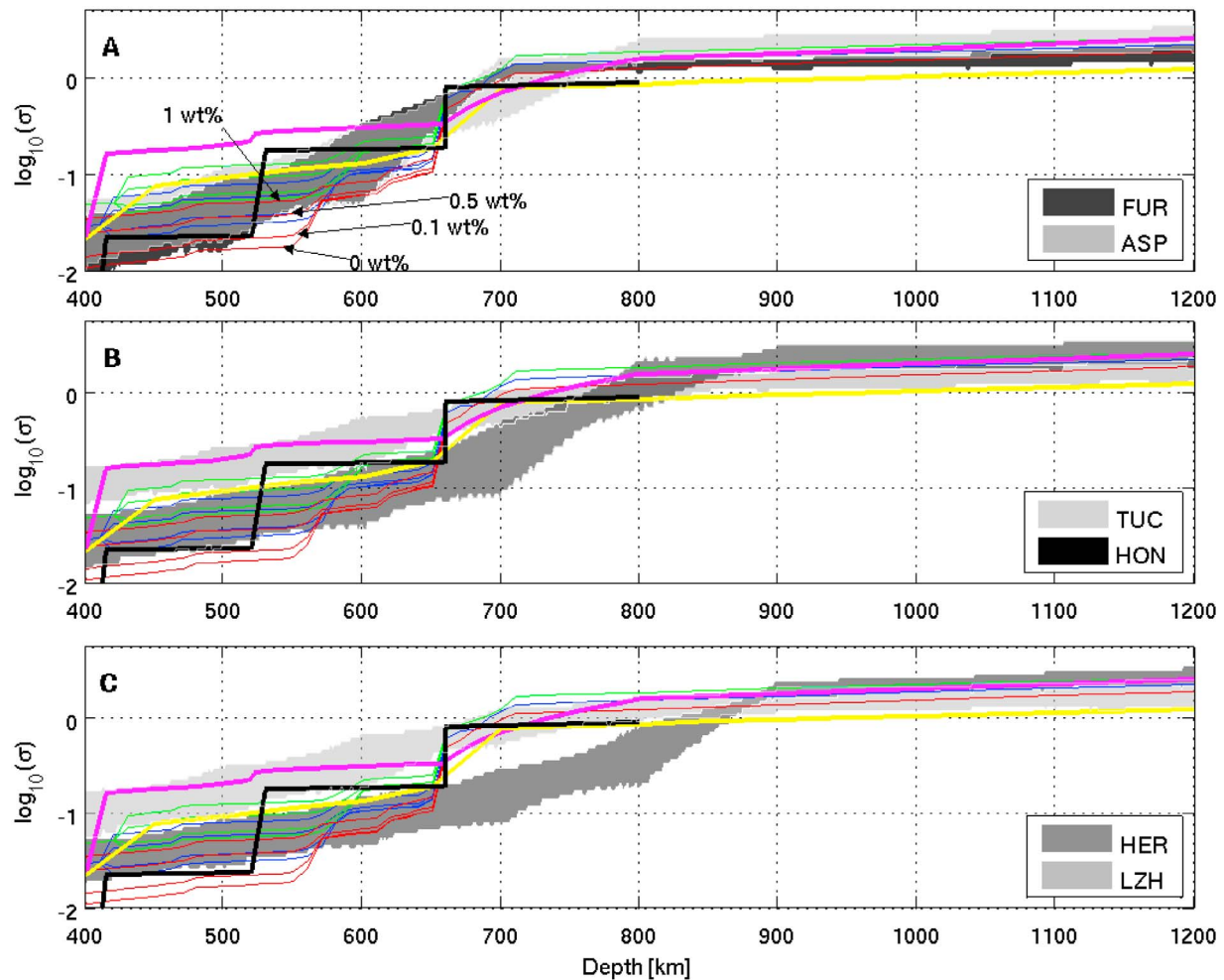


Figure 10. Comparison between inverted profiles (same as in Figure 6) and laboratory-based profiles for various adiabats (red, 1200°; blue, 1300°; green, 1400°; and transition zone water contents). For all laboratory-based profiles shown, we assume, as in Figure 9, a homogeneous pyrolitic mantle composition. For comparison, some previous laboratory-based conductivity models are shown from the studies of *Xu et al.* [2000a] (magenta), *Khan et al.* [2006] (yellow), and *Yoshino et al.* [2008a] (solid black). Note that the model by *Khan et al.* [2006] is the mean profile, and uncertainties (not shown) are typically of the order of ± 0.5 S/m, while the model of *Yoshino et al.* [2008a] was only constructed between 200 and 800 km depth.

complicates the interpretation. From Figures 10b and 10c, it is evident that for TUC and LZH, for example, only in the case of the highest water content and thermal conditions do our models barely overlap the laboratory-based profiles. However, water contents of 1 wt% are probably a bit too high as the maximum solubility of water in Ring decreases from ~ 2 wt% at 1300 K [*Inoue et al.*, 1995; *Kohlstedt et al.*, 1996] to < 0.5 wt% at ~ 1870 K [*Ohtani et al.*, 2000]. If this is indeed the case, the only other way to explain the increased conductivity beneath TUC and HER for depths < 660 km relative to the laboratory-based profiles would be to increase temperatures by another 100°C. However, such large differences in temperature are not very likely [e.g., *Ritsema et al.*, 2009; *Khan et al.*, 2006, 2009], and the observed variations in conductivity are probably influenced by compositional differences also, such as an increased Fe content resulting in a higher conductivity of Ring [*Yoshino and Katsura*, 2009a].

[47] We note that *Yoshino et al.* [2008a] inferred a dry mantle TZ from their conductivity measurements of Wads and Ring by comparing their data with the conductivity model obtained by *Kuvshinov et al.* [2005] for the North Pacific region. However, such qualitative comparisons can be misleading, in particular when uncertainties in all data parameters (i.e., EM sounding data and conductivity measurements) are not taken into account. For completeness, we should mention the model of *Kelbert et al.* [2009], which is the first global 3D electrical conductivity model of its kind. Such models hold the potential of putting constraints on the lateral variation of water content in the TZ. *Kelbert et al.* [2009] found strong evidence of high conductivity along the circum-Pacific margin, particularly beneath the western Pacific margin, where resolution was best. The high conductance was observed to extend through the depth of the TZ, which was inferred to be due to hydrated minerals that were carried down-slab into the TZ. However, the nature of

the EM sounding data used in constructing the model of *Kelbert et al.* [2009] are such that only very limited spatial resolution could be achieved, which precluded drawing firm inferences of variations in TZ water content on a global scale as also acknowledged by the authors.

[48] In the foregoing discussion, we have omitted the contribution to conductivity from the presence of melt, which can potentially increase conductivity by several orders of magnitude [e.g., *Shankland and Waff*, 1977; *Tyburczy and Waff*, 1983; *Roberts and Tyburczy*, 1999; *Gaillard*, 2004; *Yoshino et al.*, 2010]. A somewhat unconvincing attempt at modeling the effect of melt in the TZ beneath station TUC was undertaken by *Toffelmier and Tyburczy* [2007]. Their preferred conductivity model, which included the presence of a thin melt layer on top of the TZ, however, did not fit the part of the long-period magnetotelluric response functions (of *Egbert et al.* [1992]) that are mainly sensitive to upper mantle and TZ structure. This contrasts with the present findings, where data are fit over the entire period range with what are essentially melt-free models. Given the present scarcity in melt conductivity measurements, we leave it for future studies to consider these effects in more detail.

[49] In summary, while there presently is little to be said about water content in the TZ, it is clear that the observed conductivity variations between the various stations reflect important variations in temperature as well as in composition. Ascertaining the relative contributions, however, is beyond the scope of this study and can only be addressed using a more definitive approach inverting *C*-responses directly for thermo-chemical state [*Khan et al.*, 2006] and water content relying on the latest mineral physics data.

5.4. Resolution and Convergence

[50] On a more technical note, we briefly mention issues of convergence and resolution, which are important when drawing conclusions from inverse calculations. Criteria usually adopted regarding convergence, and in particular the robustness of results, include the necessity of stabilization of inverted parameter values and the similarity of these values across independent chains, which usually provide adequate confidence in the results [e.g., *Bosch*, 1999, and references therein]. We performed three independent inversions of the HER data set using three different random number sequences, and while the results (not shown) vary in detail, the general characteristics are, as expected, similar. The issue of data resolution is generally best addressed by direct comparison of prior and posterior *pdfs*, which has already been discussed. In addition, we note that the *pdfs* from the two independent runs of the HER data set have the same resolution as the “original” inversion.

6. Conclusions

[51] The purpose here has been to infer the conductivity structure beneath locations that cover a variety of geological settings using the method of EM sounding to decipher the large-scale heterogeneous structures that pervade the mantle seen in seismic tomography images. To this end, we considered a number of geomagnetic observatories and ended up with six stations located in Europe, Asia, Australia, South Africa, and North America because of the restrictions that we imposed on the quality and quantity of data. With

the exception of most European observatories, we found surprisingly few stations where 50 years of data of sufficient quality are available (our search was not exhaustive), from which a set of good-quality *C*-responses with low noise levels and high coherency could be prepared. In spite of our ambition to produce long-period *C*-responses that sample well into the lower mantle, i.e., >1500 km depth, we were limited to ~95 days, because the quality of the *C*-responses beyond these periods strongly diminished. The resulting *C*-responses are able to constrain the conductivity structure of the mantle from the TZ to 1200 km depth, with highest sensitivity in the depth range 600–1200 km.

[52] We inverted the *C*-responses beneath each of the six locations for a 1D radial conductivity profile using a stochastic sampling algorithm, obviating any linearizations and regularizations of the problem, typical of deterministic algorithms. Sampling models from the joint posterior *pdf* this were done using a MCMC sampling method, i.e., by performing a random walk in a multidimensional model space that combines prior information with information from measurements and from the theoretical relationship between data and model parameters. As output, we assimilated random realizations of the posterior *pdf*, which contains all the information about our parameterized physical system.

[53] The inversion conducted here reveals lateral variations in electrical conductivity beneath all six stations. The largest variations are found in the depth range 600–900 km, with average conductivities varying from 0.1 S/m (600 km depth) to 2.4 S/m (900 km), while differences, although somewhat diminished, persist down to 1200 km depth. At 1200 km depth, stations HER, HON, and ASP are more conductive (2.4–2.6 S/m) by almost an order of magnitude in comparison to LZH, FUR, and TUC (1.6–1.7 S/m). Throughout the depth range studied, conductivities are found to increase continuously as expected from laboratory measurements of mantle mineral electrical conductivities. Although differences in conductivity among the six stations are still present, these differences are not as strong in this region of the lower mantle as they are above 900 km depth. Comparing the results found here with models derived on the basis of mantle mineral conductivity measurements combined with mantle compositional and thermal models reveals that significant lateral variations in mantle composition, temperature, and possibly water content exist.

[54] Conclusions drawn from only six stations distributed across the globe obviously lack statistical significance, in addition to the bias introduced by the geographical distribution of selected stations. This points to the need for a continued effort to produce a global set of *C*-responses that can be used to infer mantle electrical conductivity on a global scale as initiated by *Kelbert et al.* [2009]. Since variations in conductivity with mineralogy are much stronger than the corresponding variations in elastic properties, electrical conductivity offers, in principle, a more sensitive means of probing Earth's mantle composition and thermal state. However, the somewhat large bounds on conductivity that are inferred here will likely preclude a unique determination of the relative importance of mantle compositional and thermal variations. A possible solution is to incorporate different geophysical, geodynamical, and possibly geochemical data, where available, into the inversion as a means to further reduce the inherent nonuniqueness.

[55] **Acknowledgments.** We extend our gratitude to A. Schultz and A. Jones for their very stimulating and constructive reviews. This work was supported by the Danish Agency for Science, Technology and Innovation and Swiss National Science Foundation grant 200021-130411. Finally, a part of this work was also supported by the Russian Foundation for Basic Research under grant 09-05-01071-a.

References

- Banks, R. (1969), Geomagnetic variations and the electrical conductivity of the upper mantle, *Geophys. J. R. Astron. Soc.*, *17*, 457.
- Becker, T., and L. Boschi (2002), A comparison of tomographic and geodynamic mantle models, *Geochem. Geophys. Geosyst.*, *3*(1), 1003, doi:10.1029/2001GC000168.
- Bercovici, D., and S.-I. Karato (2003), Whole-mantle convection and the transition-zone water filter, *Nature*, *425*, 39.
- Bina, C., and G. R. Helffrich (1994), Phase-transition Clapeyron slopes and transition zone seismic discontinuity topography, *J. Geophys. Res.*, *99*, 15,853, doi:10.1029/94JB00462.
- Bosch, M. (1999), Lithologic tomography: From plural geophysical data to lithology estimation, *J. Geophys. Res.*, *104*, 749, doi:10.1029/1998JB900014.
- Brown, J. M., and T. J. Shankland (1981), Thermodynamic parameters in the Earth as determined from seismic profiles, *Geophys. J. R. Astron. Soc.*, *66*, 579.
- Chave, A. D., and D. J. Thomson (2004), Bounded influence magnetotelluric response function estimation, *Geophys. J. Int.*, *157*, 988.
- Christensen, U. R., and A. W. Hofmann (1994), Segregation of subducted oceanic crust in the convecting mantle, *J. Geophys. Res.*, *99*, 19,867, doi:10.1029/93JB03403.
- Connolly, J. A. D. (2005), Computation of phase equilibria by linear programming: A tool for geodynamic modeling and an application to subduction zone decarbonation, *Earth Planet. Sci. Lett.*, *236*, 524.
- Constable, S., and C. Constable (2004), Observing geomagnetic induction in magnetic satellite measurements and associated implications for mantle conductivity, *Geochem. Geophys. Geosyst.*, *5*, Q01006, doi:10.1029/2003GC000634.
- Dai, L., and S.-I. Karato (2009), Electrical conductivity of wadsleyite at high temperatures and high pressure, *Earth Planet. Sci. Lett.*, *287*, 277, doi:10.1016/j.epsl.2009.08.012.
- Dobson, D. P., and J. P. Brodholt (2000a), The electrical conductivity and thermal profile of the Earth's mid-mantle, *Geophys. Res. Lett.*, *27*, 2325, doi:10.1029/1999GL008409.
- Dobson, D. P., and J. P. Brodholt (2000b), The electrical conductivity of the lower mantle phase magnesio-wüstite at high temperatures and pressures, *J. Geophys. Res.*, *105*, 531, doi:10.1029/1999JB900242.
- Egbert, G., and J. R. Booker (1992), Very long period magnetotellurics at Tucson observatory: Implications for mantle conductivity, *J. Geophys. Res.*, *97*, 15,099, doi:10.1029/92JB01251.
- Egbert, G., J. R. Booker, and A. Schultz (1992), Very long period magnetotellurics at Tucson observatory: Implications for mantle conductivity, *J. Geophys. Res.*, *97*, 15,113, doi:10.1029/92JB01252.
- Fujii, I., and A. Schultz (2002), The 3D electromagnetic response of the Earth to ring current and auroral oval excitation, *Geophys. J. Int.*, *151*, 689.
- Fukao, Y., T. Koyama, M. Obayashi, and H. Utada (2004), Trans-Pacific temperature field in the mantle transition region derived from seismic and electromagnetic tomography, *Earth Planet. Sci. Lett.*, *217*, 425.
- Gaillard, F. (2004), Laboratory measurements of electrical conductivity of hydrous and dry silicic melts under pressure, *Earth Planet. Sci. Lett.*, *218*, 215.
- Gamble, T. D., J. Clarke, and W. M. Goubau (1979), Magnetotellurics with a remote magnetic reference, *Geophysics*, *44*, 53.
- Hastings, W. K. (1973), Monte Carlo sampling methods using Markov chains and their applications, *Biometrika*, *57*, 97.
- Helffrich, G. R., and B. J. Wood (2001), The Earth's mantle, *Nature*, *412*, 501.
- Hirth, G., and D. L. Kohlstedt (1996), Water in the oceanic upper mantle: Implications for rheology, melt extraction and the evolution of the lithosphere, *Earth Planet. Sci. Lett.*, *144*, 93.
- Hofmann, A. W. (1997), Mantle geochemistry: The message from oceanic volcanism, *Nature*, *306*, 429.
- Huang, X., Y. Xu, and S.-I. Karato (2005), Water content in the transition zone from electrical conductivity of wadsleyite and ringwoodite, *Nature*, *434*, 746.
- Ichiki, M., M. Uyeshima, H. Utada, Z. Guoze, T. Ji, and M. Mingzhi (2001), Upper mantle conductivity structure of the back-arc region beneath northeastern China, *Geophys. Res. Lett.*, *28*, 3773, doi:10.1029/2001GL012983.
- Jones, A. G., P. Lezaeta, I. J. Ferguson, A. D. Chave, R. Evans, X. Garcia, and J. Spratt (2003), The electrical structure of the Slave craton, *Lithos*, *71*, 505.
- Jones, A. G., R. L. Evans, and D. W. Eaton (2009), Velocity-conductivity relationships for mantle mineral assemblages in Archean cratonic lithosphere based on a review of laboratory data and Hashin-Shtrikman extremal bounds, *Lithos*, *109*, 131, doi:10.1016/j.lithos.2008.10.014.
- Karato, S.-I. (2003), The role of hydrogen in the electrical conductivity of the upper mantle, *Nature*, *347*, 272.
- Karato, S.-I. (2009), Rheology of the deep upper mantle and its implications for the preservation of the continental roots: A review, *Tectonophysics*, *481*, 82, doi:10.1016/j.tecto.2009.04.011.
- Karato, S.-I., and L. Dai (2009), Comments on "Electrical conductivity of wadsleyite as a function of temperature and water content" by Manthilake et al., *Phys. Earth Planet. Inter.*, *174*, 19, doi:10.1016/j.pepi.2009.01.011.
- Katsura, T., K. Sato, and E. Ito (1998), Electrical conductivity of silicate perovskite at lower-mantle conditions, *Nature*, *395*, 493.
- Kelbert, A., A. Schultz, and G. Egbert (2009), Global electromagnetic induction constraints on transition-zone water content variations, *Nature*, *460*, 1003, doi:10.1038/nature08257.
- Khan, A., J. A. D. Connolly, and N. Olsen (2006), Constraining the composition and thermal state of the mantle beneath Europe from inversion of long-period electromagnetic sounding data, *J. Geophys. Res.*, *111*, B10102, doi:10.1029/2006JB004270.
- Khan, A., L. Boschi, and J. A. D. Connolly (2009), On mantle chemical and thermal heterogeneities and anisotropy as mapped by inversion of global surface wave data, *J. Geophys. Res.*, *114*, B09305, doi:10.1029/2009JB006399.
- Kohlstedt, D. L., H. Keppler, and D. C. Rubie (2009), Solubility of water in the α , β and γ phases of (Mg,Fe)₂SiO₄, *Contrib. Mineral. Petrol.*, *123*, 345.
- Koyama, T., H. Shimizu, H. Utada, M. Ichiki, E. Ohtani, and R. Hae (2006), Water content in the mantle transition zone beneath the North Pacific derived from the electrical conductivity anomaly, in *Earth's Deep Water Cycle*, *Geophys. Monogr. Ser.*, vol. 168, edited by S. Jacobsen and S. van der Lee, p. 171, AGU, Washington D. C.
- Kustowski, B., G. Ekström, and A. M. Dziewonski (2008), Anisotropic shear-wave velocity structure of the Earth's mantle: A global model, *J. Geophys. Res.*, *113*, B06306, doi:10.1029/2007JB005169.
- Kuvshinov, A. V. (2008), 3-D global induction in the oceans and solid Earth: Recent progress in modeling magnetic and electric fields from sources of magnetospheric, ionospheric and oceanic origin, *Surv. Geophys.*, *29*, 139.
- Kuvshinov, A., and N. Olsen (2006), A global model of mantle conductivity derived from 5 years of CHAMP, Ørsted, and SAC-C magnetic data, *Geophys. Res. Lett.*, *33*, L18301, doi:10.1029/2006GL027083.
- Kuvshinov, A. V., N. Olsen, D. B. Avdeev, and O. V. Pankratov (2002), Electromagnetic induction in the oceans and the anomalous behaviour of coastal C-responses for periods up to 20 days, *Geophys. Res. Lett.*, *29*(12), 1595, doi:10.1029/2001GL014409.
- Kuvshinov, A., H. Utada, D. Avdeev, and T. Koyama (2005), 3-D modeling and analysis of D_{st} C-responses in the North Pacific Ocean region, revisited, *Geophys. J. Int.*, *160*, 505.
- Ledo, J., and A. G. Jones (2005), Upper mantle temperature determined from combining mineral composition, electrical conductivity laboratory studies and magnetotelluric field observations: Application to the Intermontane Belt, Northern Canadian Cordillera, *Earth Planet. Sci. Lett.*, *236*, 258.
- Lizzaralde, D., A. Chave, G. Hirth, and A. Schultz (1995), Northeastern Pacific mantle conductivity profile from long-period magnetotelluric sounding using Hawaii to California submarine cable data, *J. Geophys. Res.*, *100*, 17,837, doi:10.1029/95JB01244.
- Manthilake, M., T. Matsuzaki, T. Yoshino, S. Yamashita, E. Ito, and T. Katsura (2009), Electrical conductivity of wadsleyite as a function of temperature and water content, *Phys. Earth Planet. Inter.*, *174*, 10, doi:10.1016/j.pepi.2008.06.001.
- Martinez, Z., and J. Velinsky (2009), The adjoint sensitivity method of EM induction for CHAMP magnetic data, *Geophys. J. Int.*, *179*, 1372.
- Metropolis, N., A. W. Rosenbluth, M. N. Rosenbluth, A. H. Teller, and E. Teller (1953), Equation of state calculations by fast computing machines, *J. Chem. Phys.*, *21*, 1087.

- Mosegaard, K. (1998), Resolution analysis of general inverse problems through inverse Monte Carlo sampling, *Inverse Probl.*, *14*, 405.
- Mosegaard, K., and A. Tarantola (1995), Monte Carlo sampling of solutions to inverse problems, *J. Geophys. Res.*, *100*, 12,431, doi:10.1029/94JB03097.
- Nakagawa, T., P. J. Tackley, F. Deschamps, and J. A. D. Connolly (2009), Incorporating self-consistently calculated mineral physics into thermochemical mantle convection simulations in a 3D spherical shell and its influence on seismic anomalies in Earth's mantle, *Geochem. Geophys. Geosyst.*, *10*, Q03004, doi:10.1029/2008GC002280.
- Neal, S. L., R. L. Mackie, J. C. Larsen, and A. Schultz (2000), Variations in the electrical conductivity of the upper mantle beneath North America and the Pacific Ocean, *J. Geophys. Res.*, *105*, 8229, doi:10.1029/1999JB900447.
- Ohta, K., S. Onoda, K. Hirose, R. Sinmyo, K. Shimizu, N. Sata, Y. Ohishi, and A. Yasuhara (2008), The electrical conductivity of Post-perovskite in Earth's D" Layer, *Science*, *320*, 89.
- Olsen, N. (1999), Long-period (30 days–1 year) electromagnetic sounding and the electrical conductivity of the lower mantle beneath Europe, *Geophys. J. Int.*, *138*, 179.
- Panning, M., and B. Romanowicz (2006), A three-dimensional radially anisotropic model of shear velocity in the whole mantle, *Geophys. J. Int.*, *167*, 361.
- Parker, R. L., and K. Whaler (1981), Numerical methods for establishing solutions to the inverse problem of electromagnetic induction, *J. Geophys. Res.*, *86*, 9574, doi:10.1029/JB086iB10p09574.
- Ringwood, A. E. (1975), *Composition and Petrology of the Earth's Mantle*, McGraw-Hill, New York.
- Ritsema, J. W., Xu, L., Stixrude, and C. Lithgow-Bertelloni (2009), Estimates of the transition zone temperature in a mechanically mixed upper mantle, *Earth Planet. Sci. Lett.*, *277*, 244, doi:10.1016/j.epsl.2008.10.024.
- Roberts, J. J., and J. A. Tyburczy (1991), Frequency dependent electrical properties of polycrystalline olivine compacts, *J. Geophys. Res.*, *96*, 16,205, doi:10.1029/91JB01574.
- Roberts, J. J., and J. A. Tyburczy (1999), Partial-melt conductivity: Influence of melt composition, *J. Geophys. Res.*, *104*, 7055, doi:10.1029/1998JB900111.
- Romano, C., B. Poe, N. Kreidie, and C. McCammon (2008), Electrical conductivities of pyrope-almandine garnets up to 19 GPa and 1700°C, *Am. Mineral.*, *91*, 1371.
- Schmucker, U. (1970), *Anomalies of Geomagnetic Variations in the Southwestern United States*, *Bull. Scripps Inst. Oceanogr. Ser.*, pp. 127–132, Univ. of Calif. Press, Berkeley.
- Schmucker, U. (1985a), Electrical properties of the Earth's interior, in *Landolt-Börnstein, New-Series*, 5/2b, p. 370, Springer, Berlin.
- Schmucker, U. (1985b), Magnetic and electric fields due to electromagnetic induction by external sources, in *Landolt-Börnstein, New-Series*, 5/2b, p. 100, Springer, Berlin.
- Schmucker, U. (1999), A spherical harmonic analysis of solar daily variations in the years 1964–1965: response estimates and source fields for global induction. II. Results, *Geophys. J. Int.*, *136*, 455.
- Schultz, A. (1990), On the vertical gradient and lateral heterogeneity in mid-mantle electrical conductivity, *Phys. Earth Planet. Inter.*, *64*, 68.
- Schultz, A., and J. C. Larsen (1987), On the electrical conductivity of the mid-mantle: I. Calculation of equivalent scalar magnetotelluric response functions, *Geophys. J. R. Astron. Soc.*, *88*, 733.
- Schultz, A., and J. C. Larsen (1990), On the electrical conductivity of the mid-mantle II: Delineation of heterogeneity by application of extremal inverse solutions, *Geophys. J. Int.*, *101*, 565.
- Schultz, A., R. D. Kurtz, A. D. Chave, and A. G. Jones (1993), Conductivity discontinuities in the upper mantle beneath a stable craton, *Geophys. Res. Lett.*, *20*, 2941, doi:10.1029/93GL02833.
- Shankland, T. J., and A. D. Dube (1990), Standard electrical conductivity of isotropic, homogeneous olivine in the temperature range 1200–1500°C, *Geophys. J. Int.*, *103*, 25.
- Shankland, T. J., and H. S. Waff (1977), Partial melting and electrical conductivities in the upper mantle, *J. Geophys. Res.*, *82*, 5409, doi:10.1029/JB082i033p05409.
- Shankland, T. J., J. Peyronneau, and J. P. Poirier (1993), Electrical conductivity of the Earth's lower mantle, *Nature*, *366*, 453.
- Shimizu, H., T. Koyama, K. Baba, and H. Utada (2009), Three-dimensional geomagnetic response functions for global and semi-global scale induction problems, *Geophys. J. Int.*, *178*, 123.
- Shimizu, H., H. Utada, K. Baba, T. Koyama, M. Obayashi, and Y. Fukao (2010), Three-dimensional imaging of electrical conductivity in the mantle transition zone beneath the North Pacific Ocean by a semi-global induction study, *Phys. Earth Planet. Inter.*, doi:10.1016/j.pepi.2010.01.010, in press.
- Srivastava, S. P. (1966), Theory of the magnetotelluric method for a spherical conductor, *Geophys. J. R. Astron. Soc.*, *11*, 373.
- Stacey, F. D., and O. L. Anderson (2001), Electrical and thermal conductivities of Fe-Ni-Si alloy under core conditions, *Phys. Earth Planet. Inter.*, *124*, 153.
- Tarantola, A. (2004), *Inverse Problem Theory and Methods for Model Parameter Estimation*, SIAM, Philadelphia, Pa.
- Tarantola, A., and B. Valette (1982), Inverse problems = Quest for information, *J. Geophys.*, *50*, 159.
- Tarits, P., S. Hautot, and F. Perrier (2004), Water in the mantle: Results from electrical conductivity beneath French Alps, *Geophys. Res. Lett.*, *31*, L06612, doi:10.1029/2003GL019277.
- Toffelmier, D. A., and J. A. Tyburczy (2007), Electromagnetic detection of a 410-km-deep melt layer in the southwestern United States, *Nature*, *447*, 991, doi:10.1038/nature05922.
- Trampert, J., F. Deschamps, J. Resovsky, and D. Yuen (2004), Chemical heterogeneities throughout the lower mantle, *Science*, *306*, 853.
- Trampert, J., and R. D. van der Hilst (2005), Towards a quantitative interpretation of global seismic tomography, in *Earth's Deep Mantle: Structure, Composition and Evolution*, *Geophys. Monogr. Ser.*, vol. 160, edited by R. D. van der Hilst et al., p. 47, AGU, Washington, D. C.
- Tyburczy, J. A., and D. K. Fisler (1995), Electrical properties of minerals and melts, in *Mineral Physics and Crystallography: A Handbook of Physical Constants*, edited by T. J. Ahrens, p. 185, AGU, Washington D. C.
- Tyburczy, J. A., and H. S. Waff (1983), Electrical conductivity of molten basalt and andesite to 25 kilobars pressure: Geophysical significance and implications for charge transport and melt structure, *J. Geophys. Res.*, *88*, 2413, doi:10.1029/JB088iB03p02413.
- Utada, H., T. Koyama, H. Shimizu, and A. D. Chave (2003), A semi-global reference model for electrical conductivity in the mid-mantle beneath the North Pacific region, *Geophys. Res. Lett.*, *30*(4), 1194, doi:10.1029/2002GL016092.
- Utada, H., T. Koyama, M. Obayashi, and Y. Fukao (2009), A joint interpretation of electromagnetic and seismic tomography models suggests the mantle transition zone below Europe is dry, *Earth Planet. Sci. Lett.*, *281*, 249, doi:10.1016/j.epsl.2009.02.027.
- Velimsky, J. (2010), Electrical conductivity in the lower mantle: Constraints from CHAMP satellite data by time-domain EM induction modelling, *Phys. Earth Planet. Inter.*, *180*, 111, doi:10.1016/j.pepi.2010.02.007.
- Weidelt, P. (1972), The inverse problem of geomagnetic induction, *Z. Geophys.*, *38*, 257.
- Wood, B. J. (1995), The effect of H₂O on the 410-kilometer seismic discontinuity, *Science*, *268*, 71.
- Xie, S., and P. J. Tackley (2004), Evolution of helium and argon isotopes in a convecting mantle, *Phys. Earth Planet. Inter.*, *146*, 417.
- Xu, Y., and T. J. Shankland (1999), Electrical conductivity of orthopyroxene and its high pressure phases, *Geophys. Res. Lett.*, *26*, 2645.
- Xu, Y., C. McCammon, and B. T. Poe (1998), The effect of alumina on the electrical conductivity of silicate perovskite, *Science*, *282*, 922.
- Xu, Y., T. Shankland, and B. Poe (2000a), Laboratory-based electrical conductivity in the Earth's mantle, *J. Geophys. Res.*, *105*, 27,865, doi:10.1029/2000JB900299.
- Xu, Y., T. J. Shankland, and A. G. Dube (2000b), Pressure effect on electrical conductivity of mantle olivine, *Phys. Earth Planet. Inter.*, *118*, 149.
- Yoshino, T., and T. Katsura (2009a), Effect of iron content on electrical conductivity of ringwoodite, with implications for electrical structure in the transition zone, *Phys. Earth Planet. Inter.*, *174*, 3, doi:10.1016/j.pepi.2008.09.015.
- Yoshino, T., and T. Katsura (2009b), Reply to Comments on "Electrical conductivity of wadsleyite as a function of temperature and water content" by Manthilake et al., *Phys. Earth Planet. Inter.*, doi:10.1016/j.pepi.2009.01.012.
- Yoshino, T., T. Matsuzaki, S. Yamashita, and T. Katsura (2006), Hydrous olivine unable to account for conductivity anomaly at the top of the asthenosphere, *Nature*, *443*, 973, doi:10.1038/nature05223.
- Yoshino, T., G. Manthilake, T. Matsuzaki, and T. Katsura (2008a), Dry mantle transition zone inferred from the conductivity of wadsleyite and ringwoodite, *Nature*, *451*, 326, doi:10.1038/nature06427.
- Yoshino, T., M. Nishi, T. Matsuzaki, D. Yamazaki, and T. Katsura (2008b), Electrical conductivity of majorite garnet and its implications

- for electrical structure in the mantle transition zone, *Phys. Earth Planet. Inter.*, 170, 193, doi:10.1016/j.pepi.2008.04.009.
- Yoshino, T., T. Matsuzaki, A. Shatskiy, and T. Katsura (2009), The effect of water on the electrical conductivity of olivine aggregates and its implications for the electrical structure of the upper mantle, *Earth Planet. Sci. Lett.*, 288, 291, doi:10.1016/j.epsl.2009.09.032.
- Yoshino, T., M. Laumonier, E. McIsaac, and T. Katsura (2010), Electrical conductivity of basaltic and carbonatite melt-bearing peridotites at high pressures: Implications for melt distribution and melt fraction in the upper mantle, *Earth Planet. Sci. Lett.*, 295, 593, doi:10.1016/j.epsl.2010.04.050.
-
- A. Khan, Institute of Geochemistry and Petrology and Institute of Geophysics, Swiss Federal Institute of Technology, Clausiusstrasse 25, CH-8092 Zurich, Switzerland. (amir.khan@erdw.ethz.ch)
- A. Kuvshinov and A. Semenov, Institute of Geophysics, Swiss Federal Institute of Technology, Sonneggstrasse 5, CH-8092 Zurich, Switzerland. (kuvshinov@erdw.ethz.ch; alexey.semenov@erdw.ethz.ch)